Contrib Mineral Petrol (1996) 124: 1–18 

**Huai-Jen Yang · Rosamond J. Kinzler**
**Timothy L. Grove**

# Experiments and models of anhydrous, basaltic olivine-plagioclase-augite saturated melts from 0.001 to 10 kbar

Received: 24 July 1995 / Accepted: 12 January 1996

**Abstract** A new method for modeling fractional crystallization processes that involve olivine (ol), plagioclase (plag) and augite (aug) is presented. This crystallization assemblage is the major control on the chemical variations in mid-ocean ridge basalts. The compositional and temperature variations in ol-plag-aug saturated basalts over a range of pressures are described using empirical expressions. A data base of 190 experiments in natural and basalt-analog chemical systems is used to describe temperature, Al, Ca and Mg molar fractions as functions of Si, Fe, Na, Ti and K molar fractions and pressure. Increases in the abundances of Na and K cause Ca and Mg abundances to decrease and Al abundance to increase in ol-plag-aug saturated melts. The equations can be used to predict pressure and temperature and thus provide a useful thermobarometer. A model is described to calculate ol-plag-aug fractional crystallization as a function of pressure and melt composition, using melt and augite models developed here, combined with existing models for olivine-melt and plagioclase-melt equilibria. We compare the fractional crystallization sequence of ALV-2004-3-1 predicted from the models presented in this paper, Langmuir et al. (1992) modified by Reynolds (1995), Ghiorso and Sack (1995) and Ariskin et al. (1993) at 0.001 and 4 kbar. As an example the model is applied to estimate pressure of crystallization of glasses from the east flank of the East Pacific Rise at 11°45′N.

H.-J. Yang · T.L. Grove (✉)
Department of Earth, Atmospheric and Planetary Sciences,
Massachusetts Institute of Technology,
Cambridge, MA 02139, USA

R.J. Kinzler
Lamont-Doherty Geological Observatory of Columbia University,
Palisades, NY 10964, USA

Editorial responsibility: J. Hoefs

## Introduction

Phase diagrams have been used extensively in the investigation of the generation and evolution of basalts. Phase diagrams in the simple systems, such as CaO-MgO-$Al_2O_3$-$SiO_2$ (CMAS) and CMAS+$Na_2O$, are powerful because the limited variance of equilibria in these systems allows the phase boundaries to be depicted in one, two and three dimensions, and thus easily visualized. For example, Walter and Presnall (1994) determined the position of the boundary of olivine-orthopyroxene-clinopyroxene-aluminous phase-melt in *P*-*T*-composition space by parameterizing the divariant equilibrium melting in the CMAS+$Na_2O$ system from 7 to 35 kbar in terms of pressure and $Na_2O$ abundance in the melt. Shi developed equations to describe the olivine (ol)-plagioclase (plag)-augite (aug)-melt (OPAM) boundary from experiments in the CMAS+FeO (Shi 1992) and CMAS+FeO+$Na_2O$ (Shi 1993) system at 0.001 kbar. Phase diagrams relevant for natural system crystallization and melting processes have traditionally been less tractable due to the higher variance of equilibria in the natural system. The accumulation of relevant experimental data, however, has made possible the development of methods for predicting multi-variant phase boundaries (degree of freedom greater than three). Kinzler and Grove (1992), for example, compiled ~70 experimental data to develop equations to describe the phase boundaries defined by melts coexisting with ol, aug, low-Ca pyroxene and an Al phase in both the plagioclase and spinel stability fields and Longhi (1991) provided a model for phase boundaries for hypersthene basalts.

In this study, the results of anhydrous experiments carried out at 0.001 kbar on a variety of basaltic compositions are presented. In order to explore the effects of minor components (Na, Ti, and K) on the OPAM boundary, the data presented here and from the literature are predicted using equations derived from experiments in the system CMAS+FeO (Shi 1992). Differences between observed and predicted compositions are interpreted to be caused by the presence of minor components

such as $Na_2O$, $K_2O$ and $TiO_2$ in the natural system. We then develop empirical equations constrained by the thermodynamic variance of the system describing the OPAM boundary in *P-T*-composition space, based on 190 experiments in the natural and simple systems over the pressure range of 0.001 to 10 kbar. These equations resolve the individual effects of Na, K and Ti on Ca, Al and Mg in ol-plag-aug saturated melts. We also demonstrate how to use these equations as a thermobarometer to estimate the pressure and temperature at which a given melt can be saturated with ol, plag, and aug.

Empirical equations for predicting augite composition as a function of pressure and coexisting melt composition are also presented. These equations for describing melt and augite compositions are combined with the existing parameterizations for ol-melt and plag-melt equilibria to construct a phase-diagram-based model for calculating fractional crystallization paths for a range of basaltic compositions. Software for carrying out the fractional crystallization calculations discussed in this paper is available from the authors. The model follows the philosophy of Longhi (1991) and Grove et al. (1992) by providing a quantitative prediction of the phase boundaries for a given melt composition which are then used to predict crystallization paths. This work represents an improvement over the method described by Grove et al. (1992), because composition and pressure effects on both ol-plag-aug saturated melt and augite compositions are taken into account. The OPAM boundary is especially relevant for mid-ocean ridge basalts (MORB) as the dominant geochemical variations present in MORB are attributed to ol-plag-aug fractionation (Walker et al. 1979; Stolper 1980).

## Experiments

### Starting material

The six lavas used in our experiments consist of fresh glassy to aphyric pillow fragments. Four of the lavas, PROTEA-9-70-002, 67-032, 64-002 and 61-002, were dredged from 10∼12°N on the EPR (East Pacific Rise) in 1984 (Thompson et al. 1985, 1989). The fifth, ALV-2004-3-1, was sampled by ALVIN dive 2004 at 11°45′N on the EPR. The sixth, RE-46, which has the highest MgO abundance coupled with an unusually low $Na_2O$ abundance, is an Icelandic basalt. Table 1 provides chemical analyses of the starting material. PROTEA-9-70-002 was analyzed by electron microprobes at both the Smithsonian Institution and the Massachusetts Institute of Technology (MIT).

### Experimental and analytical methods

Anhydrous isothermal experiments were carried out at 0.001 kbar. The freshest parts of the basalt pillows were reduced to powder by grinding in a SPEX shatter box for 3 minutes. About 0.08∼0.1 g of powdered sample was pressed into a pellet using elvanol as a binder. The pellet was sintered on a 0.0080 diameter Fe-Pt alloy wire loop using a natural gas/oxygen torch. The loop and sample were suspended in the hot spot of a Deltech DT31VT quenching furnace. Temperature was monitored by a Pt-$Pt_{90}Rh_{10}$ thermocouple which was calibrated against the melting points of NaCl, Au and Pt on the IPTS 1968 temperature scale (Biggar 1972). Oxygen fugacity was controlled near the quartz-fayalite-magnetite (QFM) oxygen buffer using a $CO_2$-$H_2$ gas mixture, and monitored by $ZrO_2$-CaO electrolyte cells. Experiments were terminated by quenching in water. Experimental conditions are reported in Table 2.

Volatilization of sodium from the experimental charge and mass transfer of iron between the experimental charge and container (wire loop) can be significant problems in 0.001 kbar experiments. In order to minimize the iron exchange between the silicate charge and Pt wire loop, the loops used to hold the experimental charge were fabricated to contain about 8 wt% iron. This Fe-Pt alloy is in equilibrium with tholeiite at QFM over the temperature interval of 1400 to 1100°C (Grove 1981). Sodium volatilization is related to sample size, gas flow rate, oxygen fugacity, experimental duration, and experimental temperature (Tormey et al. 1987). Larger sample size (100 mg), and low gas flow rate (0.1 ml/s) were used to reduce sodium volatilization. Mass balance between the bulk composition of starting material and experimental products was used to evaluate whether iron or sodium had been lost from the silicate charge. The $Na_2O$ loss was typically 1–5% relative. Iron loss was typically less than 1–3%.

Phase compositions were analyzed with MIT 5-spectrometer JEOL 733 Superprobe, using 15 keV accelerating voltage and 10 nA beam current. Beam size is 10 μm for glass analyses and 1 μm for crystalline phases. Counting times were 20–40 s depending on elements. The data were reduced using Bence and Albee

**Table 1** Starting compositions used in experiments

| Composition | $SiO_2$ | $TiO_2$ | $Al_2O_3$ | FeO | MgO | MnO | CaO | $K_2O$ | $Na_2O$ | $P_2O_5$ | Total |
|---|---|---|---|---|---|---|---|---|---|---|---|
| 67-032[a] | 50.2 | 1.59 | 15.8 | 9.50 | 7.52 | – | 11.6 | 0.15 | 2.88 | 0.17 | 99.4 |
| 64-002[a] | 50.2 | 1.50 | 16.1 | 9.21 | 7.91 | – | 11.9 | 0.12 | 2.68 | 0.16 | 99.8 |
| 61-002[a] | 50.4 | 1.84 | 14.7 | 10.3 | 6.96 | – | 11.7 | 0.17 | 2.90 | 0.18 | 99.2 |
| 70-002[a] | 50.2 | 1.26 | 16.0 | 9.04 | 8.24 | – | 12.5 | 0.10 | 2.50 | 0.13 | 100.0 |
| 70-002[b] | 49.6 (1) | 1.20 (2) | 15.8 (2) | 8.98 (7) | 8.66 (6) | 0.17 (3) | 11.9 (1) | 0.10 (1) | 2.67 (6) | 0.12 (4) | 99.2 |
| 70-002[c] | 50.1 | 1.22 | 15.9 | 9.07 | 8.74 | – | 12.0 | 0.10 | 2.70 | 0.12 | 100.0 |
| 70-002[d] | 49.8 | 1.25 | 15.9 | 8.96 | 8.75 | – | 12.4 | 0.10 | 2.67 | 0.13 | 100.0 |
| 2004-3-1[e] | 49.1 (2) | 1.19 (2) | 16.3 (1) | 8.65 (9) | 9.13 (5) | 0.09 (5) | 11.7 (2) | 0.10 (1) | 2.66 (14) | 0.04 (2) | 99.0 |
| RE-46 | 48.8 | 0.62 | 15.4 | 8.91 | 10.7 | 0.16 | 13.5 | 0.01 | 1.55 | 0.03 | 99.8 |

[a] Determined with the Smithsonian Institution electron microprobe

[b] Average of 368 electron microprobe analyses collected with the MIT JEOL electron microprobe, numbers in parentheses represent 1 sigma deviation in terms of least units cited, thus 49.6 (1) should be read as 49.6±0.1

[c] 70-002[b] normalized to 100%, excluding MnO

[d] 70-002[a], after the following correction factors were applied: $SiO_2$=0.9944; MgO=1.0686; $Na_2O$=1.076, and then renormalized to 100%; these correction factors were determined by comparing analyses of the same set of 8 natural glass chips collected on each microprobe, and applying corrections for oxides that were 2 sigma or greater outside of electron microprobe counting statistics

[e] As in b but average of 7 microprobe analyses

**Table 2** Experimental conditions and phase assemblages

| | Run no. | *T* °C | Log $f(O_2)$ | Time (hrs) | Run products[a] | Phase proportion (wt%) | $\Sigma R^{2b}$ |
|---|---|---|---|---|---|---|---|
| 2004-3-1 | 50 | 1223 | −8.25 | 18.6 | Gl,plag,ol | 97:2:1 | 0.77 |
| | 40 | 1213 | −8.36 | 46.0 | Gl,plag,ol | 84:12:4 | 0.70 |
| | 20 | 1188 | −8.72 | 77.8 | Gl,plag,ol | 70:22:8 | 1.04 |
| | 10 | 1170 | −8.95 | 164.2 | Gl,plag,ol,aug | 57:28:13:2 | 1.11 |
| | 60 | 1152 | −9.39 | 170.2 | Gl,plag,ol,aug | 34:40:14:13 | 0.94 |
| | 70 | 1134 | −9.24 | 166.0 | Gl,plag,ol,aug | 26:43:14:17 | 0.69 |
| 70-002 | 110 | 1160 | −8.58 | 93.5 | Gl,plag,ol | | |
| | 120 | 1152 | −9.02 | 93.5 | Gl,plag,ol,aug | 48:31:9:12 | 0.18 |
| | 130 | 1140 | −9.20 | 142.3 | Gl,plag,ol,aug | 41:34:10:15 | 0.13 |
| | 140 | 1128 | −9.38 | 165.0 | Gl,plag,ol,aug | 25:42:11:22 | 0.11 |
| 67-032 | 100 | 1191 | −8.52 | 114.3 | Gl,plag,ol | | |
| | 110 | 1171 | −8.58 | 93.5 | Gl,plag,ol,aug | 73:20:4:3 | 0.27 |
| | 130 | 1140 | −9.20 | 142.3 | Gl,plag,ol,aug | 48:32:7:13 | 0.05 |
| | 140 | 1128 | −9.38 | 165.0 | Gl,plag,ol,aug | 40:36:8:16 | 0.19 |
| | 150 | 1110 | −9.76 | 269.8 | Gl,plag,ol,aug | 29:42:9:19 | 0.51 |
| 64-002 | 100 | 1190 | −8.71 | 94.5 | Gl,plag,ol | | |
| | 110 | 1160 | −8.95 | 99.8 | Gl,plag,ol,aug | 59:28:6:7 | 0.13 |
| | 140 | 1128 | −9.40 | 166.3 | Gl,plag,ol,aug | 40:36:8:16 | 0.19 |
| | 150 | 1110 | −9.66 | 218.5 | Gl,plag,ol,aug | 23:47:10:20 | 0.34 |
| 61-002 | 100 | 1190 | −8.71 | 94.5 | Gl,plag,ol | | |
| | 110 | 1160 | −8.95 | 99.8 | Gl,plag,ol,aug | 80:14:4:2 | 0.05 |
| | 130 | 1140 | −9.14 | 146.5 | Gl,plag,ol,aug | 64:22:3:11 | 0.07 |
| | 140 | 1128 | −9.38 | 165.0 | Gl,plag,ol,aug | 48:30:5:15 | 0.92 |
| | 150 | 1110 | −9.66 | 218.5 | Gl,plag,ol,aug | 35:36:6:22 | 0.13 |
| RE-46 | 10 | 1251 | −8.39 | 136.2 | Gl | | |
| | 15 | 1251 | −7.90 | 6.5 | Gl | | |
| | 5 | 1245 | −8.42 | 6.2 | Gl | | |
| | 4 | 1230 | −8.53 | 23.5 | Gl,ol | 99:1 | 1.02 |
| | 9 | 1225 | −8.44 | 121.5 | Gl,plag,ol | 93:4:3 | 0.93 |
| | 14 | 1207 | −8.48 | 95.8 | Gl,plag,ol | 86:8:6 | 0.19 |
| | 8 | 1198 | −8.80 | 164.3 | Gl,plag,ol,aug | 71:16:8:4 | 0.51 |
| | 7 | 1170 | −9.31 | 183.0 | Gl,plag,ol,aug | 41:31:11:17 | 0.37 |

[a] Abbreviation used: *Gl* glass, *ol* olivine, *plag* plagioclase, *aug* augite

[b] Sum of the residuals squared for an unweighted least squares fit of the run product compositions to the starting composition

(1968) matrix correction with modification of Albee and Ray (1970). The compositions of the phases in the experiments are listed in Table 3.

### Attainment of equilibrium

The experiments described here were all synthesis experiments. Reversal experiments were not conducted and therefore equilibrium has not been demonstrated with respect to all possible exchange components. Several lines of observation indicate that the experiments closely approached equilibrium. First, the Fe-Mg bearing crystalline phases show generally consistent partitioning with respect to iron and magnesium. The Fe-Mg exchange distribution coefficients $[K_D=(X_{Fe}^{xtl}\cdot X_{Mg}^{liq})/(X_{Mg}^{xtl}\cdot X_{Fe}^{liq})]$ are $0.28\pm0.01$ for olivine-liquid and $0.24\pm0.02$ for augite-liquid. Similarly, the plagioclase-liquid Ca-Na exchange distribution coefficients $[K_D=(X_{Ca}^{xtl}\cdot X_{Na}^{liq})/(X_{Na}^{xtl}\cdot X_{Ca}^{liq})]$ range from 0.75 to 1.30. The consistent $K_D$ values are as expected from other phase equilibrium studies and provide evidence for an approach to equilibrium. Second, replicate analyses of glasses and olivines show that these phases are homogeneous within the precision of the electron microprobe analytical technique. Individual augite and plagioclase analyses often vary outside the practical analytical reproducibility described above. The presence of sector zoning and small-scale heterogeneities in composition are inconsistent with attainment of total equilibrium. To achieve totally homogeneous phases, the experiments would need to have been longer than those carried out here (up to 270 hours) and this was not practical, because other factors (e.g., Na loss) begin to compromise the experimental results. Thus, the experiments were run as long as practically possible to achieve homogeneous products, but were limited by Na loss from the sample, which has the undesirable effect of changing compositions of solid and melt phases.

## Experimental results

The crystallization sequence for sample RE-46 is olivine followed by plagioclase then augite in at 1198°C (Fig. 1). Sample ALV-2004-3-1 has olivine and plagioclase as liquidus phases followed by augite in at 1170°C. Augite

**Table 3** Compositions of experimental products. Paranthesized units represent 1 sigma of replicate analyses in terms of least units cited. Thus, 49.7 (1) should be read as 49.7 ±0.1

| Run | Phase | No. of analyses | $SiO_2$ | $TiO_2$ | $Al_2O_3$ | FeO | MgO | MnO | CaO | $K_2O$ | $Na_2O$ | $P_2O_5$ | Total |
|---|---|---|---|---|---|---|---|---|---|---|---|---|---|
| 2004-3-1-50 | Gl | 7 | 49.7 (1) | 1.18 (2) | 16.4 (1) | 8.78 (12) | 9.00 (10) | 0.15 (2) | 11.8 (2) | 0.10 (1) | 2.53 (10) | 0.04 (1) | 99.7 |
| | Ol | 3 | 50.5 (3) | 0.0 | 0.09 (2) | 12.3 (2) | 46.9 (5) | 0.10 (1) | 0.50 (1) | – | – | – | 100.3 |
| | Plag | 3 | 49.6 (6) | – | 31.8 (6) | 0.55 (5) | 0.30 (6) | – | 15.5 (2) | 0.02 (1) | 2.68 (11) | – | 100.4 |
| 2004-3-1-40 | Gl | 7 | 50.2 (2) | 1.38 (6) | 15.4 (2) | 9.46 (10) | 8.35 (7) | 0.14 (4) | 12.0 (1) | 0.11 (2) | 2.63 (11) | 0.04 (1) | 99.7 |
| | Ol | 3 | 39.9 (4) | 0.0 | 0.12 (4) | 14.1 (2) | 45.8 (2) | 0.17 (1) | 0.47 (2) | – | – | – | 100.6 |
| | Plag | 4 | 49.3 (1) | – | 31.7 (1) | 0.65 (4) | 0.30 (7) | – | 15.7 (1) | 0.02 (1) | 2.59 (6) | – | 100.3 |
| 2004-3-1-20 | Gl | 6 | 50.2 (3) | 1.58 (4) | 14.2 (9) | 9.84 (13) | 7.71 (12) | 0.19 (7) | 12.3 (1) | 0.14 (1) | 2.64 (21) | 0.04 (1) | 98.8 |
| | Ol | 3 | 39.7 (4) | 0.03 (1) | 0.12 (3) | 15.3 (1) | 43.9 (2) | 0.28 (1) | 0.50 (1) | – | – | – | 99.7 |
| | Plag | 4 | 50.3 (9) | – | 29.8 (11) | 0.95 (22) | 0.54 (24) | – | 14.9 (4) | 0.03 (1) | 2.91 (21) | – | 99.4 |
| 2004-3-1-10 | Gl | 6 | 50.8 (3) | 2.17 (10) | 13.5 (2) | 11.0 (1) | 7.08 (7) | 0.27 (2) | 11.5 (1) | 0.17 (2) | 2.52 (2) | 0.11 (5) | 99.2 |
| | Ol | 4 | 39.6 (5) | 0.05 (1) | 0.08 (2) | 18.1 (6) | 42.1 (5) | 0.31 (3) | 0.46 (3) | – | – | – | 100.7 |
| | Plag | 4 | 50.7 (4) | – | 29.9 (4) | 0.71 (11) | 0.40 (10) | – | 14.4 (2) | 0.04 (1) | 3.23 (8) | – | 99.4 |
| | Aug | 8 | 51.5 (1.1) | 0.72 (21) | 2.92 (78) | 6.36 (88) | 16.7 (6) | 0.16 (4) | 20.8 (2) | – | 0.21 (6) | – | 99.3 |
| 2004-3-1-60 | Gl | 10 | 50.4 (4) | 3.33 (20) | 12.5 (2) | 12.9 (3) | 6.22 (13) | 0.22 (3) | 10.4 (2) | 0.25 (1) | 2.51 (9) | 0.48 (6) | 99.4 |
| | Ol | 4 | 38.8 (1) | 0.07 (4) | 0.06 (4) | 22.8 (2) | 38.7 (2) | 0.36 (3) | 0.41 (3) | – | – | – | 101.2 |
| | Plag | 3 | 52.3 (5) | – | 29.5 (4) | 0.75 (4) | 0.36 (18) | – | 13.5 (3) | 0.03 (2) | 3.83 (17) | – | 100.3 |
| | Aug | 13 | 51.8 (4) | 0.94 (14) | 2.46 (57) | 7.94 (36) | 16.4 (5) | 0.12 (4) | 19.8 (3) | – | 0.26 (6) | – | 99.7 |
| 2004-3-1-70 | Gl | 10 | 50.0 (7) | 4.14 (44) | 12.1 (5) | 13.4 (7) | 5.75 (3) | 0.23 (3) | 10.0 (2) | 0.28 (3) | 2.55 (12) | 0.54 (5) | 99.0 |
| | Ol | 5 | 38.5 (4) | 0.10 (1) | 0.06 (5) | 24.9 (12) | 36.9 (9) | 0.38 (1) | 0.45 (2) | – | – | – | 101.3 |
| | Plag | 3 | 52.3 (5) | – | 29.1 (1) | 0.78 (8) | 0.30 (5) | – | 13.4 (3) | 0.02 (2) | 3.88 (22) | – | 99.8 |
| | Aug | 7 | 51.3 (7) | 1.28 (29) | 2.86 (72) | 8.89 (81) | 16.3 (6) | 0.18 (6) | 18.8 (11) | – | 0.32 (13) | – | 99.9 |
| 70-002-120 | Gl | 9 | 50.1 (4) | 2.52 (13) | 13.4 (1) | 11.9 (1) | 6.30 (6) | 0.16 (3) | 10.8 (1) | 0.38 (2) | 3.31 (9) | 0.19 (3) | 99.1 |
| | Ol | 6 | 38.9 (3) | 0.04 (3) | 0.38 (26) | 20.8 (1) | 39.9 (3) | 0.35 (2) | 0.53 (6) | – | – | – | 100.9 |
| | Plag | 6 | 52.5 (8) | – | 29.2 (6) | 0.86 (11) | 0.32 (5) | – | 13.2 (6) | 0.11 (3) | 3.90 (33) | – | 100.1 |
| | Aug | 10 | 51.7 (1.1) | 1.10 (49) | 2.84 (82) | 7.29 (1.4) | 15.7 (1.2) | 0.13 (4) | 20.6 (4) | – | 0.28 (7) | – | 99.6 |
| 70-002-130 | Gl | 9 | 50.3 (8) | 2.80 (3) | 13.2 (3) | 12.2 (6) | 5.90 (15) | 0.28 (11) | 10.3 (3) | 0.45 (4) | 3.25 (21) | 0.25 (7) | 98.9 |
| | Ol | 5 | 38.5 (2) | 0.00 | 0.19 (4) | 23.4 (3) | 38.0 (2) | 0.37 (1) | 0.29 (17) | – | – | – | 100.8 |
| | Plag | 5 | 51.9 (9) | – | 29.4 (2) | 0.70 (10) | 0.27 (4) | – | 13.4 (3) | 0.10 (1) | 3.75 (7) | – | 99.5 |
| | Aug | 8 | 52.1 (2) | 0.96 (13) | 2.48 (3) | 8.06 (29) | 16.3 (4) | 0.21 (7) | 19.5 (4) | – | 0.21 (4) | – | 99.8 |
| 70-002-140 | Gl | 8 | 49.2 (3) | 4.17 (26) | 12.0 (2) | 14.3 (3) | 5.51 (13) | 0.30 (5) | 9.90 (16) | 0.32 (6) | 2.68 (21) | 0.37 (5) | 98.7 |
| | Ol | 5 | 37.4 (2) | 0.03 (3) | 0.21 (5) | 26.4 (3) | 35.5 (2) | 0.41 (2) | 0.42 (2) | – | – | – | 100.4 |
| | Plag | 3 | 53.2 (3) | – | 28.9 (1) | 0.73 (9) | 0.22 (3) | – | 12.8 (2) | 0.13 (1) | 4.07 (22) | – | 100.1 |
| | Aug | 4 | 51.0 (1.5) | 1.27 (27) | 3.14 (11) | 9.70 (1.4) | 15.2 (1.2) | 0.24 (5) | 18.0 (6) | – | 0.31 (8) | – | 98.9 |
| 67-032-110 | Gl | 8 | 50.4 (6) | 2.10 (21) | 13.5 (2) | 11.7 (3) | 7.05 (18) | 0.22 (4) | 11.5 (3) | 0.17 (3) | 2.66 (21) | 0.26 (6) | 99.6 |
| | Ol | 5 | 38.8 (3) | 0.00 | 0.21 (10) | 19.6 (4) | 41.2 (4) | 0.29 (4) | 0.39 (6) | – | – | – | 100.5 |
| | Plag | 4 | 50.9 (3) | – | 30.2 (6) | 0.75 (22) | 0.34 (16) | – | 14.6 (3) | 0.08 (1) | 3.11 (15) | – | 100.0 |
| | Aug | 7 | 52.5 (1) | 0.74 (25) | 2.47 (61) | 6.59 (70) | 16.9 (4) | 0.17 (5) | 19.9 (3) | – | 0.21 (5) | – | 99.5 |

**Table 3** (continued)

| Run | Phase | No. of analyses | $SiO_2$ | $TiO_2$ | $Al_2O_3$ | FeO | MgO | MnO | CaO | $K_2O$ | $Na_2O$ | $P_2O_5$ | Total |
|---|---|---|---|---|---|---|---|---|---|---|---|---|---|
| 67-032-130 | Gl | 7 | 50.4 (5) | 2.62 (11) | 13.0 (2) | 13.0 (2) | 5.85 (17) | 0.27 (4) | 10.4 (2) | 0.29 (5) | 3.16 (18) | 0.23 (5) | 99.2 |
| | Ol | 5 | 38.1 (2) | 0.00 | 0.22 (7) | 22.8 (3) | 38.0 (5) | 0.39 (4) | 0.50 (7) | – | – | – | 100.0 |
| | Plag | 4 | 53.7 (7) | – | 28.3 (4) | 0.88 (10) | 0.31 (6) | – | 12.4 (4) | 0.15 (1) | 4.26 (23) | – | 100.0 |
| | Aug | 9 | 49.5 (2.2) | 1.74 (77) | 3.91 (1.47) | 9.43 (1.37) | 13.9 (1.9) | 0.23 (8) | 20.2 (4) | – | 0.37 (10) | – | 99.3 |
| 67-032-140 | Gl | 7 | 49.8 (6) | 3.56 (14) | 12.6 (1) | 13.4 (2) | 5.31 (9) | 0.31 (7) | 9.70 (16) | 0.57 (8) | 3.38 (13) | 0.34 (7) | 99.0 |
| | Ol | 5 | 37.8 (2) | 0.08 (5) | 0.22 (5) | 25.8 (4) | 35.6 (2) | 0.43 (1) | 0.52 (14) | – | – | – | 100.5 |
| | Plag | 3 | 53.8 (1) | – | 28.4 (2) | 0.63 (2) | 0.18 (1) | – | 12.0 (2) | 0.18 (0) | 4.54 (1) | – | 99.7 |
| | Aug | 10 | 50.6 (1.7) | 1.42 (46) | 3.16 (1.20) | 9.47 (1.42) | 14.8 (1.4) | 0.22 (5) | 19.9 (9) | – | 0.31 (6) | – | 99.9 |
| 67-032-150 | Gl | 9 | 49.8 (4) | 4.92 (9) | 11.7 (2) | 14.2 (3) | 4.70 (3) | 0.21 (3) | 8.88 (17) | 0.68 (5) | 3.32 (13) | 0.45 (9) | 98.9 |
| | Ol | 5 | 37.1 (2) | 0.08 (6) | 0.21 (7) | 29.0 (2) | 33.3 (3) | 0.45 (5) | 0.45 (14) | – | – | – | 100.6 |
| | Plag | 3 | 53.7 (3) | – | 27.9 (5) | 0.97 (4) | 0.66 (60) | – | 11.8 (3) | 0.17 (1) | 4.42 (8) | – | 99.6 |
| | Aug | 8 | 51.2 (6) | 1.50 (15) | 2.28 (38) | 10.2 (5) | 15.6 (5) | 0.24 (2) | 18.1 (6) | – | 0.23 (3) | – | 99.4 |
| 64-002-110 | Gl | 8 | 50.2 (2) | 2.30 (29) | 13.4 (2) | 11.9 (5) | 6.76 (27) | 0.22 (6) | 11.2 (3) | 0.22 (2) | 3.03 (18) | 0.26 (4) | 99.5 |
| | Ol | 5 | 38.9 (2) | 0.00 | 0.21 (8) | 19.1 (4) | 41.4 (2) | 0.31 (3) | 0.45 (3) | – | – | – | 100.4 |
| | Plag | 4 | 52.8 (7) | – | 28.3 (5) | 1.14 (14) | 0.53 (7) | – | 13.3 (5) | 0.10 (1) | 3.74 (27) | – | 99.9 |
| | Aug | 17 | 51.8 (8) | 0.76 (21) | 2.83 (66) | 6.70 (91) | 16.6 (7) | 0.15 (6) | 20.1 (5) | – | 0.27 (11) | – | 99.2 |
| 64-002-140 | Gl | 11 | 49.3 (2) | 3.92 (7) | 11.8 (1) | 14.0 (1) | 5.43 (4) | 0.28 (1) | 9.59 (12) | 0.35 (1) | 2.93 (7) | 0.36 (1) | 97.9 |
| | Ol | 5 | 37.3 (1) | 0.06 (4) | 0.18 (8) | 26.6 (3) | 35.3 (2) | 0.41 (5) | 0.41 (4) | – | – | – | 100.3 |
| | Plag | 4 | 53.3 (2) | – | 28.5 (4) | 0.80 (20) | 0.25 (9) | – | 12.6 (2) | 0.14 (1) | 4.14 (7) | – | 99.7 |
| | Aug | 4 | 51.5 (1.1) | 1.17 (25) | 2.57 (63) | 9.16 (69) | 15.9 (6) | 0.18 (5) | 18.9 (2) | – | 0.25 (5) | – | 99.6 |
| 64-002-150 | Gl | 7 | 48.4 (5) | 5.28 (18) | 11.2 (2) | 15.4 (4) | 4.99 (3) | 0.23 (4) | 9.40 (4) | 0.43 (3) | 2.76 (13) | 0.49 (7) | 98.6 |
| | Ol | 5 | 36.8 (3) | 0.05 (7) | 0.20 (4) | 29.2 (2) | 33.2 (2) | 0.46 (3) | 0.44 (1) | – | – | – | 100.5 |
| | Plag | 4 | 54.1 (6) | – | 27.8 (1.0) | 0.85 (22) | 0.47 (41) | – | 12.0 (3) | 0.17 (2) | 4.50 (7) | – | 99.9 |
| | Aug | 9 | 51.4 (3) | 1.36 (10) | 2.05 (23) | 9.92 (24) | 15.6 (2) | 0.19 (6) | 18.4 (4) | – | 0.26 (4) | – | 99.2 |
| 61-002-110 | Gl | 8 | 50.4 (6) | 2.27 (18) | 13.3 (4) | 11.9 (6) | 6.71 (35) | 0.23 (7) | 11.2 (2) | 0.19 (3) | 2.73 (21) | 0.26 (8) | 99.2 |
| | Ol | 5 | 38.7 (3) | 0.00 | 0.17 (4) | 19.2 (3) | 41.2 (5) | 0.26 (8) | 0.44 (3) | – | – | – | 100.0 |
| | Plag | 3 | 52.1 (3) | – | 28.4 (5) | 1.12 (18) | 0.56 (10) | – | 13.7 (3) | 0.10 (1) | 3.53 (17) | – | 99.5 |
| | Aug | 8 | 52.3 (5) | 0.72 (5) | 2.50 (29) | 6.40 (43) | 17.0 (1) | 0.15 (5) | 20.2 (3) | – | 0.24 (4) | – | 99.5 |
| 61-002-130 | Gl | 7 | 50.0 (7) | 2.98 (48) | 12.8 (4) | 13.1 (5) | 6.06 (16) | 0.28 (6) | 10.5 (34) | 0.31 (3) | 2.91 (15) | 0.26 (4) | 99.2 |
| | Ol | 5 | 38.3 (3) | 0.00 | 0.20 (6) | 23.8 (3) | 37.9 (3) | 0.35 (3) | 0.45 (4) | – | – | – | 101.0 |
| | Plag | 4 | 53.3 (6) | – | 28.7 (7) | 0.87 (31) | 0.29 (14) | – | 12.9 (2) | 0.12 (0) | 4.09 (14) | – | 100.3 |
| | Aug | 8 | 52.6 (8) | 0.81 (9) | 2.29 (44) | 7.86 (34) | 16.8 (3) | 0.24 (2) | 19.2 (4) | – | 0.22 (3) | – | 100.0 |
| 61-002-140 | Gl | 7 | 49.8 (4) | 3.33 (31) | 12.2 (3) | 14.3 (4) | 5.29 (23) | 0.25 (6) | 9.73 (40) | 0.37 (4) | 3.08 (21) | 0.32 (6) | 98.7 |
| | Ol | 5 | 37.4 (2) | 0.10 (5) | 0.28 (8) | 27.5 (4) | 34.3 (4) | 0.44 (2) | 0.49 (7) | – | – | – | 100.5 |
| | Plag | 4 | 54.8 (4) | – | 28.2 (8) | 0.94 (31) | 0.24 (13) | – | 12.2 (2) | 0.13 (1) | 4.38 (14) | – | 100.9 |
| | Aug | 5 | 52.1 (4) | 0.94 (7) | 2.17 (37) | 8.91 (27) | 15.9 (2) | 0.18 (2) | 18.4 (3) | – | 0.27 (2) | – | 98.9 |

**Table 3** (continued)

| Run | Phase | No. of analyses | $SiO_2$ | $TiO_2$ | $Al_2O_3$ | FeO | MgO | MnO | CaO | $K_2O$ | $Na_2O$ | $P_2O_5$ | Total |
|---|---|---|---|---|---|---|---|---|---|---|---|---|---|
| 61-002-150 | Gl | 8 | 49.2 (2) | 4.33 (12) | 11.4 (1) | 15.8 (2) | 4.74 (3) | 0.26 (4) | 9.16 (10) | 0.43 (1) | 3.02 (11) | 0.44 (4) | 98.8 |
| | Ol | 5 | 36.7 (4) | 0.16 (6) | 0.24 (6) | 31.3 (3) | 31.5 (4) | 0.47 (5) | 0.45 (1) | – | – | – | 100.8 |
| | Plag | 3 | 55.0 (2) | – | 27.9 (2) | 0.78 (5) | 0.16 (2) | – | 11.3 (1) | 0.17 (1) | 4.85 (8) | – | 100.2 |
| | Aug | 20 | 50.8 (1.0) | 1.43 (3) | 2.69 (94) | 10.5 (1.0) | 14.7 (9) | 0.24 (5) | 18.7 (7) | – | 0.30 (7) | – | 99.4 |
| RE 46-15 | Gl | 6 | 49.1 (2) | 0.50 (2) | 15.1 (1) | 8.15 (13) | 10.6 (1) | 0.10 (5) | 13.7 (2) | 0.01 (0) | 1.48 (9) | 0.08 (0) | 98.9 |
| RE 46-5 | Gl | 5 | 49.3 (2) | 0.50 (2) | 15.1 (2) | 8.21 (22) | 10.6 (1) | 0.10 (5) | 13.8 (1) | 0.01 (1) | 1.47 (9) | 0.08 (3) | 99.2 |
| RE 46-4 | Gl | 7 | 49.3 (2) | 0.53 (3) | 15.1 (1) | 8.20 (9) | 10.4 (1) | 0.08 (4) | 13.9 (2) | 0.01 (1) | 1.46 (11) | 0.07 (3) | 99.1 |
| | Ol | 4 | 40.4 (4) | 0.02 (0) | 0.06 (0) | 11.6 (2) | 47.6 (5) | 0.21 (2) | 0.40 (2) | – | – | – | 100.6 |
| RE 46-9 | Gl | 18 | 50.0 (3) | 0.55 (3) | 15.2 (2) | 8.52 (14) | 10.1 (2) | 0.18 (4) | 14.1 (1) | 0.01 (1) | 1.14 (7) | 0.12 (2) | 100.0 |
| | Ol | 4 | 40.7 (3) | 0.03 (6) | 0.09 (6) | 11.4 (2) | 48.5 (1) | 0.15 (2) | 0.41 (4) | – | – | – | 101.5 |
| | Plag | 3 | 46.8 (3) | – | 31.4 (1.0) | 1.31 (40) | 1.55 (47) | – | 17.8 (3) | 0.00 | 1.07 (2) | – | 99.9 |
| RE 46-14 | Gl | 6 | 50.1 (2) | 0.58 (1) | 14.8 (1) | 9.17 (9) | 9.43 (6) | 0.10 (4) | 14.1 (1) | 0.02 (1) | 1.42 (5) | 0.10 (2) | 99.9 |
| | Ol | 4 | 40.0 (4) | 0.02 (1) | 0.05 (0) | 13.0 (1) | 46.1 (4) | 0.24 (2) | 0.46 (2) | – | – | – | 100.1 |
| | Plag | 8 | 47.2 (3) | – | 33.4 (5) | 0.69 (11) | 0.45 (13) | – | 17.6 (2) | 0.00 | 1.37 (7) | – | 100.7 |
| RE 46-17 | Gl | 9 | 50.5 (3) | 0.68 (2) | 14.1 (1) | 9.57 (13) | 9.04 (17) | 0.14 (4) | 14.1 (1) | 0.03 (1) | 1.58 (8) | 0.12 (3) | 99.9 |
| | Ol | 3 | 40.5 (2) | – | 0.04 (0) | 13.6 (2) | 45.2 (3) | 0.20 (1) | 0.51 (3) | – | – | – | 100.4 |
| | Plag | 4 | 46.9 (4) | – | 32.8 (3) | 0.68 (07) | 0.51 (16) | – | 17.6 (1) | – | 1.32 (7) | – | 99.7 |
| RE 46-8 | Gl | 6 | 51.2 (1) | 0.80 (5) | 14.0 (1) | 10.1 (1) | 8.81 (8) | 0.19 (6) | 13.4 (1) | 0.03 (1) | 1.46 (12) | 0.11 (3) | 100.1 |
| | Ol | 8 | 40.1 (3) | 0.01 (1) | 0.07 (3) | 14.8 (3) | 45.2 (2) | 0.19 (4) | 0.46 (5) | – | – | – | 100.9 |
| | Plag | 5 | 47.2 (4) | – | 33.4 (3) | – | 0.36 (3) | – | 17.4 (2) | 0.03 (2) | 1.43 (13) | – | 100.4 |
| | Cpx | 10 | 53.2 (5) | 0.21 (2) | 2.56 (38) | 4.87 (21) | 18.4 (3) | 0.13 (2) | 21.1 (6) | – | 0.15 (2) | – | 101.4 |
| RE 46-16 | Gl | 8 | 51.3 (5) | 0.85 (4) | 14.00 (3) | 11.0 (2) | 8.00 (12) | 0.21 (4) | 12.7 (1) | 0.04 (1) | 1.80 (10) | 0.12 (2) | 100.0 |
| | Ol | 4 | 39.1 (3) | 0.03 (1) | 0.22 (2) | 17.5 (2) | 41.9 (2) | 0.31 (2) | 0.46 (3) | – | – | – | 99.9 |
| | Plag | 4 | 48.4 (7) | – | 31.4 (4) | 1.08 (07) | 0.69 (10) | – | 16.6 (4) | – | 1.80 (21) | – | 99.9 |
| | Cpx | 12 | 51.8 (3) | 0.27 (4) | 2.85 (56) | 6.41 (69) | 17.1 (3) | 0.15 (2) | 20.5 (4) | – | 0.16 (4) | – | 99.8 |
| RE 46-7 | Gl | 11 | 52.0 (2) | 1.15 (3) | 13.3 (1) | 12.2 (2) | 7.31 (22)[a] | 0.22 (7) | 12.0 (2) | 0.02 (1) | 1.61 (9) | 0.14 (9) | 100.0 |
| | Ol | 5 | 38.7 (3) | 0.02 (1) | 0.17 (5) | 20.0 (2) | 40.9 (3) | 0.30 (3) | 0.44 (4) | – | – | – | 100.7 |
| | Plag | 10 | 48.9 (1.2) | – | 31.2 (8) | 0.95 (9) | 0.50 (13) | – | 15.9 (6) | 0.02 (1) | 2.18 (34) | – | 99.6 |
| | Cpx | 8 | 51.7 (8) | 0.27 (2) | 2.38 (56) | 6.84 (34) | 17.6 (4) | 0.17 (2) | 19.7 (5) | – | 0.16 (3) | – | 99.1 |

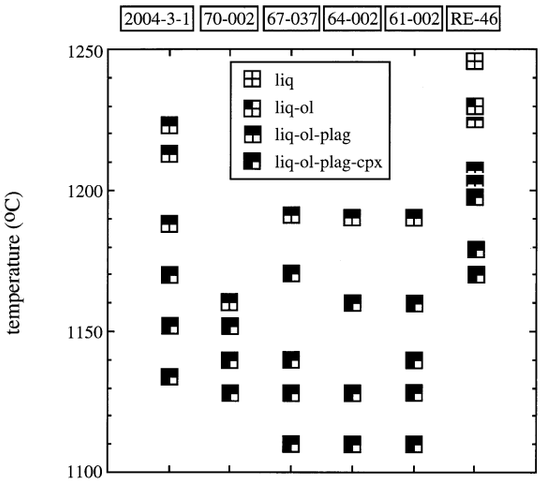


**Fig. 1** The crystallization sequence of experiments at 0.001 kbar

begins to crystallize in addition to olivine and plagioclase over the temperature interval of 1170–1150°C in the other four starting compositions. The higher ol-plag saturation temperature for RE-46 is a result of its higher $CaO/Al_2O_3$ ratio. Composition RE-46 also has a higher ol-plag-aug saturation temperature than the other compositions (Fig. 1).

## Discussion

### Prediction of ol-plag-aug saturated melts

#### *Effects of $Na_2O$*

Since 85∼90% of the chemical constituents in basalts are contained in the CMAS system, it constitutes a good analog system for studying partial melting and crystal fractionation (Presnall et al. 1978; Libourel et al. 1989). In the natural system at least four more components: FeO, $Na_2O$, $TiO_2$ and $K_2O$, are required to describe the compositional variations. Shi and Libourel (1991) carried out experiments in the CMAS+FeO system at 0.001 kbar to investigate the effects of FeO. Shi (1992) developed empirical equations to describe the compositions of ol-plag-aug saturated melts in the CMAS+FeO system at 0.001 kbar (thermodynamic variance, $F=2$). He used temperature and Si molar fraction in melt ($X_{Si}$; in later discussion $X$ denotes molar fraction of the oxide) as two independent variables to describe the molar fractions of Al, Ca, Fe and Mg ($X_{Al}$, $X_{Ca}$, $X_{Fe}$ and $X_{Mg}$) in melts saturated with ol-plag-aug. In order to evaluate the effects of $Na_2O$, $TiO_2$ and $K_2O$ on ol-plag-aug saturated melts, we used the equations of Shi (1992) to predict the compositions of melts in experiments in the CMAS+FeO+$Na_2O$ and natural systems. The data set used for evaluation is listed in Table 4 and includes experiments performed at 0.001 kbar. The comparisons between observed melt compositions and melt compositions predicted from the equations of Shi (1992) are shown in Fig. 2. Predicted melt compositions have higher $X_{Fe}$ and $X_{Ca}$, and lower $X_{Al}$ than observed compositions. Predictions for $X_{Mg}$ are good for high-Mg melts but more scattered for low-Mg melts which contain greater abundances of $Na_2O$, $TiO_2$ and $K_2O$.

The differences between observed compositions and those predicted from the equations of Shi (1992) are attributed to the effects of the minor components present in the natural system but not in CMAS+FeO. Because Na is the most abundant of the minor components in our data set [1.32∼8.43 wt%, excluding the experiments on lunar samples (Grove and Vaniman 1978)], we plot $Na_2O$ wt% against the differences between predicted and observed melt compositions (i.e., ΔAl=predicted $X_{Al}$ - ob-

**Table 4** Data used in OPAM modeling

| Source | System | *P* (kbar) | *T* (°C) | No. of experiment |
|---|---|---|---|---|
| Grove et al. 1992 | Natural | 0.001 | 1161 | 1 |
| | | 2 | 1126–1163 | 5 |
| | | 8 | 1210–1265 | 10 |
| | | 10 | 1235–1250 | 2 |
| Tormey et al. 1987 | Natural | 0.001 | 1152–1171 | 7 |
| Grove and Bryan 1983 | Natural | 0.001 | 1137–1193 | 22 |
| Grove et al. 1990 | Natural | 0.001 | 1108–1152 | 4 |
| | | 8 | 1189 | 1 |
| Juster et al. 1989 | Natural | 0.001 | 1150–1180 | 4 |
| Grove and Vaniman 1978 | Natural | 0.001 | 1099–1155 | 4 |
| Baker and Eggler 1987 | Natural | 0.001 | 1100–1175 | 6 |
| | | 8 | 1200–1250 | 4 |
| | | 2 | 1020–1060 | 3 |
| Walker et al. 1979 | Natural | 0.001 | 1085–1235 | 11 |
| Bender et al. 1978 | Natural | 8 | 1250 | 1 |
| Sack et al. 1987 | Natural | 0.001 | 1064–1176 | 20 |
| This study | Natural | 0.001 | 1110–1171 | 16 |
| Presnall et al. 1978 | CMAS | 0.001 | 1266–1272 | 2 |
| Libourel et al. 1989 | CMAS | 0.001 | 1244–1275 | 24 |
| Shi and Libourel 1991 | CMAS+FeO | 0.001 | 1160–1220 | 27 |
| Shi 1993 | CMAS+FeO+$Na_2O$ | 0.001 | 1100 | 16 |

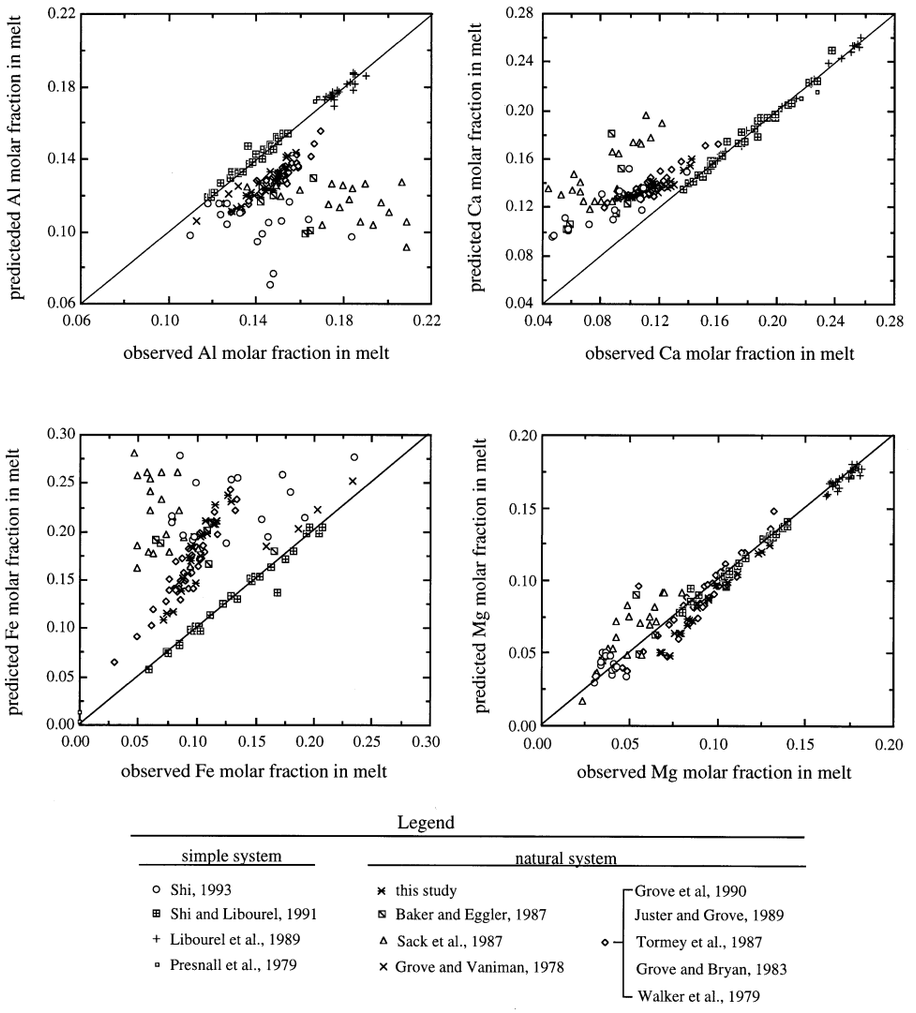


**Fig. 2** Observed ol-plag-aug saturated melt compositions versus those predicted from Shi's equations (1992). The *solid lines* indicate observed =predicted compositions

served $X_{Al}$). The $Na_2O$ correlates with ΔAl, ΔCa and ΔFe (Fig. 3). Differences increase as $Na_2O$ abundance in the melt increases. Based on Fig. 3, the addition of $Na_2O$ increases Al and decreases Ca and Fe relative to the $Na_2O$-free system. The behavior is consistent with the experimental results of Biggar and Humphries (1981). They showed that an increase in the abundance of $Na_2O$ moves ol-plag-aug saturated melt compositions towards the plagioclase apex of the forsterite-diopside-plagioclase pseudoternary in the forsterite-diopside-anorthite-albite system. Shifting ol-plag-aug saturated melt compositions towards the plagioclase apex causes increases in the Al and Si abundances and decreases in the Fe, Ca and Mg abundances in the melt. However, this plagioclase effect is difficult to reconcile with the lack of $Na_2O$-ΔMg correlation for the experiments of Shi (1993) for which $Na_2O$ is the only additional component. The Shi (1993) experiments were carried out at a constant temperature, 1100°C, and thus temperature may be exercising an important control on the $Na_2O$-ΔMg systematics. Another striking feature of the ΔMg-$Na_2O$ variation is that experiments on alkalic compositions (open triangles) and tholeiitic compositions (stars and open diamonds) do not show the systematic variation as defined by $Na_2O$ versus ΔAl, ΔCa and ΔFe. For example, the differences between predicted and observed Al, Ca and Fe increase as $Na_2O$ abundance increases from tholeiitic to alkalic compositions. In contrast, there is no systematic $Na_2O$-ΔMg variation from tholeiitic to alkalic compositions.

### *Combined effects of $TiO_2$ and $K_2O$*

The combined effects of other minor components on ol-plag-aug saturated melts can be evaluated by comparing ΔCa, ΔFe, ΔMg and ΔAl between the natural and CMAS+FeO+$Na_2O$ systems again using the equations of Shi (1992). In Fig. 3 at a given $Na_2O$ content, experimental melts of natural compositions (symbols other than open circle) have larger magnitudes of ΔCa, ΔFe and ΔAl than melts of CMAS+FeO+$Na_2O$ compositions

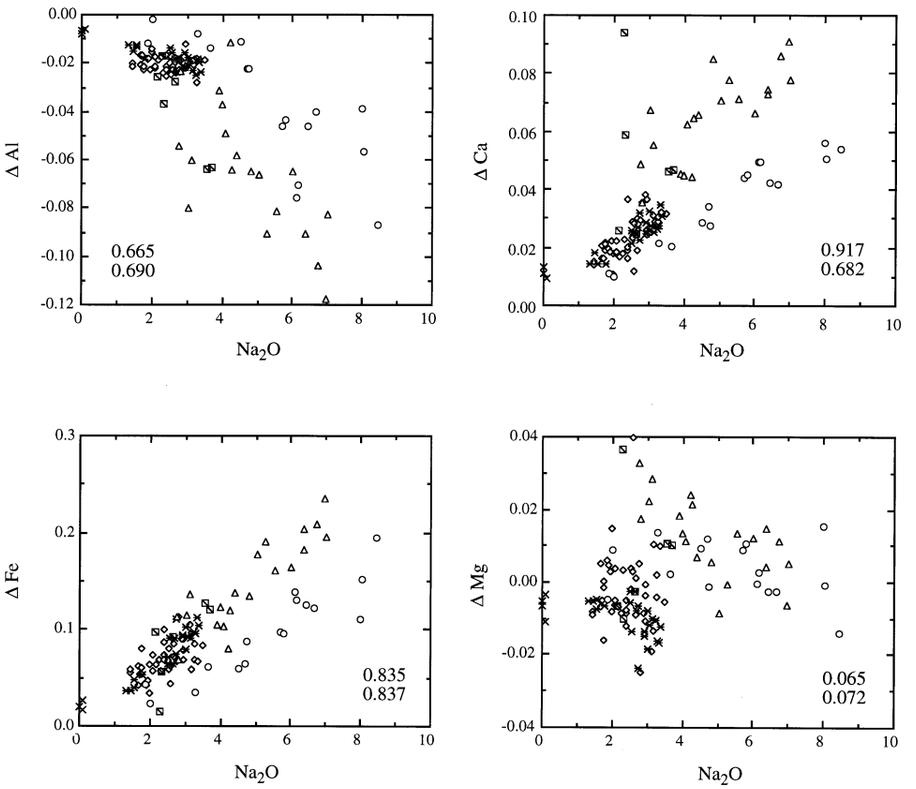


**Fig. 3** Differences between predicted and observed ol-plag-aug saturated melt compositions versus $Na_2O$ (wt%) in melt (Δ=predicted – observed). Predicted compositions are calculated from Shi's equations (1992). Symbols are the same as Fig. 2. In each panel the *upper number* is the $R^2$ for *open circles*, the experiments in the CMAS+FeO+$Na_2O$ system (Shi 1993), and the *lower number* is that for the other symbols including experiments in the natural system

(open circles). These differences can be inferred to reflect the combined effects of other minor components. As $Ti_2O$ and $K_2O$ are the next most abundant components after $Na_2O$, the discrepancies of ΔCa, ΔFe and ΔAl between the natural and CMAS+FeO+$Na_2O$ systems are attributed to the combined effects of these two elements. As Fig. 3 shows, the combined effects of $Ti_2O$ and $K_2O$ on Ca, Fe and Al abundances in ol-plag-aug saturated melts are similar to those of $Na_2O$, since the addition of $TiO_2$ and $K_2O$ increases the magnitudes of ΔCa, ΔFe and ΔAl. This analysis does not, however, allow us to distinguish between the individual effects of $TiO_2$ and $K_2O$.

### *Estimating the compositions of ol-plag-aug saturated melts*

As discussed above, variations in the abundances of minor components such as $Na_2O$, $TiO_2$ and $K_2O$ have systematic effects on the compositions of natural system melts saturated with ol-plag-aug, relative to melts saturated with this same mineral assemblage in compositionally less complex systems. We developed equations based on experiments in both the natural and the simple systems to describe the compositions of ol-plag-aug saturated melts. Data from high pressure experiments (Grove et al. 1992; Grove et al. 1990; Baker and Eggler 1987; Bender et al. 1978) were also included in the data set to parameterize equations for ol-plag-aug saturated melt compositions as functions of pressure, and bulk composition by multiple regression. This data set (Table 4) covers nepheline- and hypersthene-normative compositions, and its compositional ranges are: Mg#[Mg/(Mg+Fe)] = 0.15∼1, $Na_2O$: 0∼8.43 wt%, $SiO_2$ = 38.59 ∼63.41 wt%, $TiO_2$ = 0∼5.63 wt%, $K_2O$ = 0∼5.45 wt% and pressure ranges from 0.001 to 10 kbar. Eight components: $SiO_2$, $TiO_2$, $Al_2O_3$, FeO, MgO, CaO, $Na_2O$ and $K_2O$; are sufficient to describe melt compositions. The variance of a 4-phase equilibrium in an 8-component system is 6 ($F=C+2-\phi=8+2-4=6$; $F$ is the variance, $C$ is the number of components and $\phi$ is the number of phases). To evaluate the effects of pressure and minor components on major components, pressure, $X_{Na}$, $X_K$ and $X_{Ti}$ are chosen as independent variables. Two more independent variables are required. Least squares multiple linear regression analysis was used to obtain equations that combine $X_{Si}$ and $X_{Fe}$ with $X_{Na}$, $X_K$, $X_{Ti}$ and pressure to predict $X_{Al}$, $X_{Ca}$, $X_{Mg}$ and temperature. Using 190 experimental constraints, the coefficients for the independent variables listed in Table 5 provide the best fits describing $X_{Al}$ (Eq. 1), $X_{Ca}$ (Eq. 2), $X_{Mg}$ (Eq. 3) and temperature (Eq. 4). Pressure is in kbar and temperature is in °C. The values in parentheses are the standard errors of the coefficients. The ratio of a coefficient and its standard error ($t$-value) gives the degree of significance of its corresponding variable. The higher the absolute $t$-value is, the more significant the variable. For example, the absolute $t$-value of $X_K$ in Eq. 1 (Table 5) is 17.3 and removing the

**Table 5** Coefficients of independent variables for describing $X_{Al}$, $X_{Ca}$, $X_{Mg}$ and $T$ in ol-plag-aug saturated melt

| Eq. no. | | Constant | $P$ | $X_{Na}$ | $X_K$ | $X_{Ti}$ | $X_{Fe}$ | $X_{Si}$ | $(X_{Si})^2$ | $X_{Si}*X_{Ti}$ | $R$ |
|---|---|---|---|---|---|---|---|---|---|---|---|
| 1 | $X_{al}$ | 0.236 | 0.00218 | 0.109 | 0.593 | −0.350 | −0.299 | −0.130 | 0.0 | 0.0 | 0.937 |
| | | (0.005) | (0.00016) | (0.014) | (0.034) | (0.043) | (0.008) | (0.011) | | | |
| 2 | $X_{Ca}$ | 1.133 | −0.00339 | −0.569 | −0.776 | −0.672 | −0.214 | −3.355 | 2.830 | 0.0 | 0.982 |
| | | (0.047) | (0.00021) | (0.018) | (0.046) | (0.061) | (0.010) | (0.197) | (0.206) | | |
| 3 | $X_{Mg}$ | −0.277 | 0.00114 | −0.543 | −0.947 | −0.117 | −0.490 | 2.086 | −2.400 | 0.0 | 0.989 |
| | | (0.031) | (0.00014) | (0.012) | (0.030) | (0.040) | (0.007) | (0.131) | (0.137) | | |
| 4 | $T$ | 581.7 | 5.858 | −691.0 | −848.9 | 11492 | 3114 | −574.3 | −3529 | −25679 | 0.937 |
| | | (99.5) | (0.436) | (39.2) | (96.1) | (1582) | (416) | (21.7) | (433) | (3352) | |

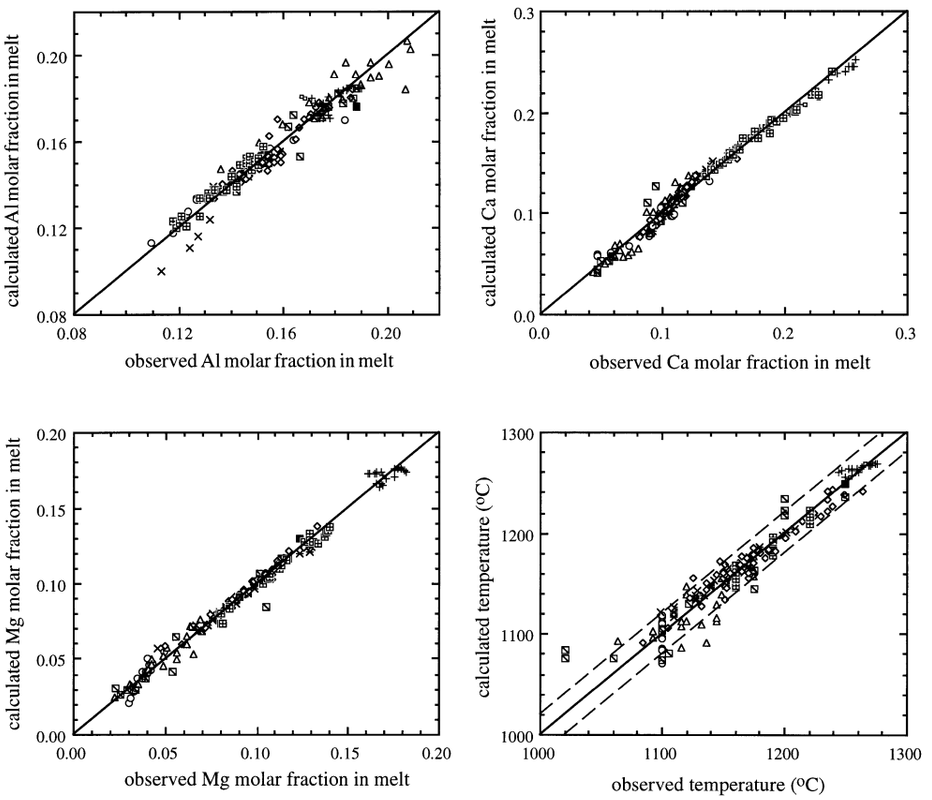


**Fig. 4** Observed compositions and temperature versus those predicted from Eqs. 1–4. Data source is listed in Table 4. Symbols for 0.001 kbar experiments are the same as Fig. 2. High pressure experiments of Grove et al. (1992) (*diamond*) and Baker and Eggler (1987) (*square with slash*) are included. The *solid square* is the 8 kbar experiment of Bender et al. (1978). The *dashed lines* in temperature plot indicate region wherein the data are fit to ±20°C

$X_K$ term from Eq. 1 decreases the square of the correlation coefficient ($R^2$) from 0.937 to 0.835. In our equations most of the variables have absolute *t*-values greater than 10. The predicted temperatures are within ±20°C of the experimental temperatures for 170 experiments. Fifteen exceed ±20°C but are less than ±30°C. Five exceed ±30°C (Fig. 4).

As Eqs. 1–3 (Table 5) are first degree polynomials for $P$, $X_{Na}$, $X_K$ and $X_{Ti}$, the individual effects of these independent variables on dependent variables can be predicted from the sign of the coefficient of that independent variable. For example, if $X_K$, $X_{Ti}$, $X_{Si}$, $X_{Fe}$ and $P$ are fixed, increasing $X_{Na}$ will decrease $X_{Ca}$ and $X_{Mg}$ but increase $X_{Al}$. Following this approach, we infer that the effects of $X_K$ on $X_{Ca}$, $X_{Mg}$ and $X_{Al}$ are the same as that of $X_{Na}$ and the effects of $X_{Ti}$ are to decrease $X_{Al}$ and $X_{Ca}$. The effect of $X_{Ti}$ on $X_{Mg}$ cannot be predicted from Eq. 3, because the absolute *t*-value of $X_{Ti}$ is 2.925 which means that $X_{Ti}$ is insignificant. Removing $X_{Ti}$ from Eq. 3 only slightly decreases $R^2$ (from 0.989 to 0.987). In order to better evaluate the effect of $X_{Ti}$ on $X_{Mg}$, we tested combinations of other independent variables to predict $X_{Mg}$ that give more significant t-value ($\sim$5.8) for $X_{Ti}$. Although these efforts led to equations with slightly low $R^2$, all predict that increasing $X_{Ti}$ will increase $X_{Mg}$ if other independent variables are fixed. Therefore, the effect of $X_{Ti}$ on $X_{Mg}$ is opposite to that of $X_{Na}$ and $X_K$. The overall effects of increasing the abundance of $X_{Ti}$ are to increase $X_{Mg}$ but

decrease $X_{Al}$ and $X_{Ca}$. These effects tend to move melt compositions away from the plagioclase apex. In summary, the effects of $X_{Na}$ and $X_K$ counterbalance the effect of $X_{Ti}$ on $X_{Mg}$. This may explain the success of the simple system equation (Shi 1992) in predicting $X_{Mg}$ (Fig. 2) for natural system data even though they did not consider the effects of $X_{Na}$, $X_K$ and $X_{Ti}$.

## Melt composition as a thermobarometer

In applying the technique described below for thermobarometric purposes or to model MORB fractional crystallization, it is necessary to correct basalt compositions for interlaboratory analytical differences. Analytical differences are known to exist among electron microprobe laboratories that commonly provide analyses of MORB glasses, which often form the starting point for models. An interlaboratory comparison has been made (Reynolds 1995) including MIT, the Smithsonian Institution in Washington, Lamont Doherty and University of Hawaii. It is the practice in our laboratory to correct microprobe data obtained elsewhere to an MIT reference before making thermobarometric or modeling analyses (see Table 1). Although Grove et al. (1992) neglected to discuss this issue, the Smithsonian data discussed in that paper was corrected before plotting and estimation of crystallization pressure. Failure to do so can result in significant errors, and is most commonly evident as a discrepancy in the pressures estimated from the different equations.

The equations presented in Table 5 can be used to estimate the temperature and pressure at which a basaltic melt may have coexisted with olivine, plagioclase and augite from the melt composition. Sample VG-360, inferred to have been on the ol-plag-aug cotectic at 4 kbar (Gataeni et al. 1995), is taken as an example. The $X_{Ca}$, $X_{Al}$ and $X_{Mg}$ predicted for VG-360 from Eqs. 1–3 at various pressures were combined with other observed components and recalculated into normative oxygen unit components (Grove et al. 1993). A series of "predicted" compositions were projected from plagioclase onto the ol-cpx-qtz plane. Comparison between the observed composition and the predicted melts indicates that the best fit is at 4 kbar (Fig. 5). Projections from ol, cpx and qtz also give best fits at 4 kbar implying that VG-360 may have been ol-plag-aug saturated at 4 kbar. Thus, the method described here gives a similar result to that obtained by Gataeni et al. (1995). The predicted pressure and compositional variables were then used in Eq. 4 to predict temperature. The predicted temperature for VG-360 is 1184°C, while prediction from olivine composition gives 1161°C (Gaetani et al. 1995). Another example shown in Fig. 5 is RE-46, a starting composition in this study. Our prediction is consistent with the experimental results presented in this study which show that RE-46 is not ol-plag-aug saturated at 0.001 kbar. The third example is the composition of the glassy matrix of SU-46-66, a dredged tholeiite from the east rift of Mauna Kea, Hawaii. Predicted and observed normative oxygen unit components match very well at 0.001 kbar. Sample SU-46-66 contains crystals of olivine, plagioclase and augite.

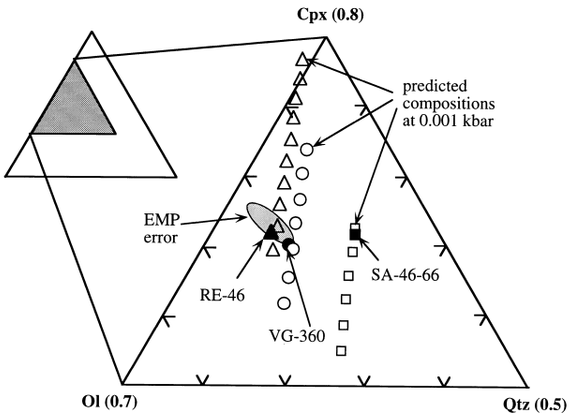


**Fig. 5** Prediction of pressures at which melts coexist with ol-plag-aug. *Solid symbols* are observed compositions. *Open symbols* are compositions predicted from Eqs. 1–3 at various pressures. For all three samples the first predicted composition is at 0.001 kbar, then, 1 kbar, 2 kbar, 3 kbar and so on. The best fits between observed and predicted compositions are at 0.001, 4, and 9 kbar for SA-46-66, VG-360 and RE-46, respectively. The 2 sigma error ellipse (*EMP error*) is calculated as standard deviation of the mean of replicate electron microprobe analyses of ALV-1690-20 starting composition (Grove et al. 1992)

## Predicting fractional crystallization paths

The equations presented in Table 5 track the position of the OPAM boundary in pressure, temperature and composition space as fractional crystallization of a basaltic magma proceeds and therefore provide the basis for a model of fractional crystallization. Grove et al. (1992) predicted the ol-plag-aug-low Ca pyroxene-melt (OPALM) point with the equations of Kinzler and Grove (1992), and then extended a straight line from the predicted OPALM point towards the Ol-Cpx sideline in the olivine-clinopyroxene-quartz (Ol-Cpx-Qtz) pseudoternary with a slope parallel to the experimentally determined OPAM boundary of ALV-1690-20 at 0.001 kbar. This was a simplification of more complex relations that are sensitive to both composition and pressure. In this paper the OPAM boundary is modeled as a function of both bulk composition and pressure. Mineral-melt equilibrium expressions for ol, plag and aug are required in order to calculate fractionation paths for melts that will saturate with some combinations of these mineral phases. As both pressure and system composition may change as fractionation proceeds, these mineral-melt equilibrium expressions need to incorporate the controls of both pressure and system composition on the compositions of ol, plag and aug that crystallize from basaltic melts.

Based on experimental results, the geometric relation between the OPALM, OPAM and ol-plag-melt (OPM) boundaries was simplified by Grove et al. (1992) in the following way. For a given pressure and bulk composition, the OPAM boundary projects as a line terminated by the OPALM point in the Ol-Cpx-Qtz pseudoternary (Fig. 6a). In the olivine-plagioclase-clinopyroxene (Ol-Plag-Cpx) pseudoternary, the OPAM line collapses as a point overlapping with the OPALM point forming the end point of the OPM boundary (Fig. 6b). The OPM boundary projects as a line perpendicular to the Ol-Plag sideline (Fig. 6b). We will use these geometric relations to predict fractionation paths. The Ol-Cpx-Qtz pseudoternary is chosen to demonstrate the OPAM boundary since the OPAM boundary appears as a prominent feature in this projection. In the following section we provide a method for predicting ol-plag-aug fractionation paths as functions of pressure and system composition.

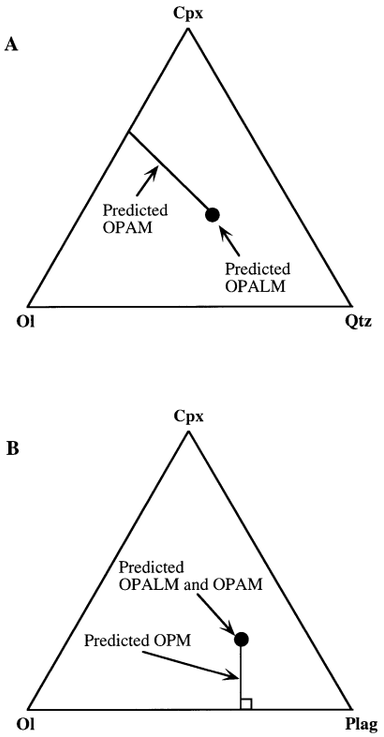


**Fig. 6 A,B** Simplified geometric relation between the OPALM, OPAM and OPM boundaries by Grove et al. (1992). The OPALM is predicted with the equations of Kinzler and Grove (1992). In Ol-Cpx-Qtz pseudoternary (**A**), OPAM is a line extended from OPALM towards Ol-Cpx sideline with a slope parallel to the experimentally determined OPAM of ALV-1690–20 at 0.001 kbar. In Ol-Cpx-Plag pseudoternary (**B**), OPAM plots as a point and overlaps with OPALM. The OPM is a line extended from OPAM (also OPALM) perpendicular to Ol-Plag sideline

*Olivine fractionation*

For MORB the most common fractionation sequence at low pressure is olivine followed by olivine-plagioclase then olivine-plagioclase-augite. A typical primitive MORB composition lies in the olivine primary phase liquidus volume. Therefore, olivine is the liquidus phase. In each fractionation step, the olivine composition can be calculated from the melt composition and the olivine-liquid Fe-Mg exchange distribution coefficient [$K_D = 0.30 \pm 0.03$]. This exchange $K_D$ is constant over the range of compositions and pressures considered in this study (Roeder and Emslie 1970; Gee and Sack 1988; Ulmer 1989). Fractionation of olivine alone proceeds until the melt composition reaches the ol-plag boundary.

*Olivine-plagioclase fractionation*

Plagioclase joins olivine as a crystallizing phase when the melt composition reaches the OPM boundary. In the Ol-Plag-Cpx pseudoternary the OPM boundary is extended from the OPALM point, which is predicted from the equations of Kinzler and Grove (1992). The intersection of the Ol-Plag sideline and the OPM boundary gives the relative proportions of olivine and plagioclase in the fractionating assemblage. The predicted OPM boundary shifts slightly as melt composition changes and the boundary is recalculated at each increment by recalculating the OPALM point for the fractionated liquid. The result is that the olivine proportions vary in a range from $30 \sim 26$ wt%. Equilibrium plagioclase compositions are calculated using the composition and pressure dependent expressions for plag-melt equilibrium of Grove et al. (1992).

*Determining melt composition for augite saturation*

For each increment in the "modeled" ol-plag fractionation path, $X_{Ca}$, $X_{Al}$ and $X_{Mg}$ were predicted by Eqs. 1–3 (Table 5), combined with other components and recalculated to form a "predicted path" of ol-plag-aug saturated melt compositions in the Ol-Cpx-Qtz pseudoternary. When the "predicted" composition for the ol-plag-aug saturated melt matches the "modeled" composition of the ol-plag saturated melt (i.e., the intersection of "modeled" ol-plag fractionation path and "predicted path", Fig. 7), augite joins the fractionating assemblage of the modeled melt. Henceforth, the fractionation assemblage contains three phases: ol, plag and aug. As an example, the first ol-plag-aug saturated melts at various pressures are shown in Fig. 7 along with "modeled" and "predicted" paths using the most primitive glass recovered from the east flank of the overlapping spreading center at 11°45′N on the EPR, ALV-2004-3-1.

*Predicting augite compositions*

Augite composition is required in order to model crystallization along the OPAM boundary. We have chosen to model experimentally produced augite compositions empirically, because none of the published models ade-

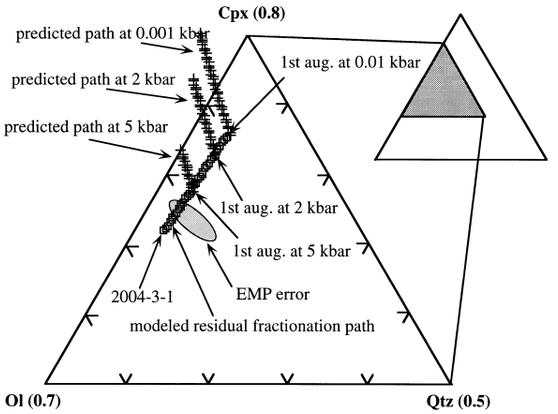


**Fig. 7** Prediction of the first ol-plag-aug saturated melt evolving from sample ALV-2004-3-1 at 0.001, 2 and 5 kbar. Modeled residual fractionation path and predicted path are described in text. The intersections of modeled residual fractionation path and predicted path indicate melt compositions first saturated with ol-plag-aug at various pressures. The *EMP error ellipse* is described in Fig. 5

quately reproduce natural system augites (Nielsen et al. 1988; Sack and Carmichael 1984; Shi 1993). We limited our calibration data set to include only augite compositions that coexist with ol-plag-aug saturated melts. The data set for regression includes experiments on natural samples over the pressure range from 0.001 to 10 kbar (Table 4). Augite composition was parameterized in terms of the composition of its coexisting melt, temperature and pressure. Combinations of independent variables that yield the best fits to 102 experimental augites are provided in Table 6. The $X_{Fe}$ and $X_{Mg}$ were combined as one dependent variable, $X_{FeMg}$, for regression. The $X_{Fe}$ and $X_{Mg}$ were then determined from the augite-melt Fe-Mg exchange $K_D$. The experimentally determined $K_D$ is 0.24 at 0.001 kbar (this study) and 0.27 at $8 \sim 10$ kbar (Grove et al. 1992). The $X_{Al}$ in augite (Eq. 10) is calculated from the other components in augite.

### *Olivine-plagioclase-augite fractionation*

In addition to mineral compositions, phase proportions are also required to constrain crystallization along the OPAM boundary. Recognizing that the OPAM boundary, as simplified by Grove et al. (1992), projects to a point in the Ol-Plag-Cpx pseudoternary and assuming that the OPAM boundary is linear in composition space, one approach is to obtain the proportions of ol-plag-aug in the crystallizing assemblage from the position of this point, relative to the projected positions of the three crystallizing phases in an oxygen-normalized projection. The predicted first ol-plag-aug saturated melt gives the ol-plag-aug proportions for the first increment of ol-plag-aug fractionation. After removing this increment, the residual melt composition is projected again onto the Ol-Plag-Cpx pseudoternary, the composition of the coexisting augite is determined and the proportions of crystallizing

**Table 6** Coefficients of independent variables for describing augite compositions coexisting with olivine, plagioclase and a basaltic melt. Independent variables in Eqs. 5–9 are melt components whereas those in Eq. 10 are augite components calculated from Eqs. 5–9. The values in parentheses are the standard errors of the coefficients.

| Eq. no. | | Constant | $P$ | $T$ | $X_{Si}$ | $X_{Ti}$ | $X_{Al}$ | $X_{Fe}$ | $X_{Mg}$ | $X_{Ca}$ | $X_{Na}$ | $X_K$ | $R^2$ |
|---|---|---|---|---|---|---|---|---|---|---|---|---|---|
| 5 | $XCa^{aug}$ | 25.043 | 0 | 0 | 0 | 0 | −0.617 | −0.832 | −0.953 | 1.624 | 0.446 | 0.446 | 0.873 |
| | | (1.473) | – | – | – | – | (0.077) | (0.047) | (0.075) | (0.086) | (0.057) | (0.057) | |
| 6 | $XMgFe^{aug}$ | −11.051 | 0 | 0 | 0.504 | 0 | 0.385 | 1.089 | 1.171 | −1.058 | 0 | 0 | 0.878 |
| | | (4.304) | – | – | (0.044) | – | (0.103) | (0.067) | (0.071) | (0.100) | – | – | |
| 7 | $XTi^{aug}$ | −3.612 | −0.0217 | 0.001052 | 0 | 0.320 | 0.108 | 0.0339 | 0 | 0.0225 | 0.0426 | 0.0426 | 0.904 |
| | | (0.557) | (0.0059) | (0.00043) | – | (0.023) | (0.021) | (0.0064) | – | (0.0149) | (0.0114) | (0.0114) | |
| 8 | $XNa^{aug}$ | −2.296 | 0 | 0.00221 | 0 | 0 | 0 | 0 | −0.0202 | 0 | 0.082 | 0 | 0.826 |
| | | (0.384) | – | (0.00040) | – | – | – | – | (0.0092) | – | (0.007) | – | |
| 9 | $XSi^{aug}$ | 116.08 | 0.204 | −0.0111 | −0.310 | −1.374 | −1.582 | −0.533 | 0 | −0.706 | −0.418 | 0 | 0.803 |
| | | (17.78) | (0.046) | (0.005) | (0.144) | (0.253) | (0.210) | (0.120) | – | (0.190) | (0.136) | – | |
| 10 | $XAl^{aug}$ | 98.236 | 0 | 0 | −0.964 | −0.799 | 0 | −1.022 | −0.998 | −1.015 | −0.932 | 0 | 0.998 |
| | | (0.690) | – | – | (0.015) | (0.045) | – | (0.016) | (0.017) | (0.014) | (0.059) | – | |

phases are estimated for the next fractionation increment. In each fractionation increment $X_{Ca}$, $X_{Al}$ and $X_{Mg}$ of residual melt are predicted by Eqs. 1–3, then combined with other modeled components to recalculate into predicted compositions. The "predicted" and "residual" compositions should match well for a self-consistent model of ol-plag-aug crystallization along the OPAM boundary, however, this was not always the case. The difference arises because the tangent of a point on the OPAM curve in the Ol-Plag-Cpx-Qtz pseudoquaternary does not intersect the Ol-Plag-Cpx pseudoternary in the same place as the projection of that point and the positions of tangent intersection changes as melts progress along the OPAM boundary. In other words the OPAM boundary is curved. Therefore, to obtain the proportions of ol-plag-aug crystallizing along the OPAM boundary we used an iterative technique. An initial estimate of ol-plag-aug proportions is chosen using the estimates of Grove et al. (1992). The compositions of residual melts are compared to predicted melts that are obtained using this first estimate of phase proportions. The proportions of ol, plag and aug are then varied until the difference between the predicted and residual compositions is minimized. The OPALM point is also predicted for each fractionation increment. The OPAM boundary terminates when it coincides with the OPALM point. The OPAM boundary modeled from an experimentally produced ol-plag-aug saturated melt, ALV-2004-3-1-10, is shown in Fig. 8 with that predicted from the method of Grove et al. (1992). Our new model provides a better fit to the experimentally determined OPAM boundary than the previous model (Grove et al. 1992).

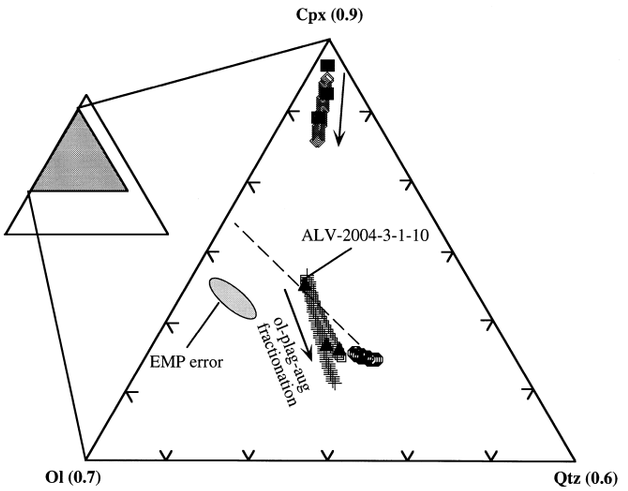


**Fig. 8** Predicting OPAM boundary from an experimentally produced ol-plag-aug saturated melt, ALV-2004-3-1-10 at 0.001 kbar. Each increment is 1 wt% fractionation. Methods for modeling are described in text. *Open squares* form the "residual" ol-plag-aug fractionation path. *Crosses* form the "predicted" OPAM path and *open circles* form the predicted OPALM path (see text for discussion). *Open diamonds* are the augite compositions predicted from the coexisting residual ol-plag-aug saturated melts. *Solid triangles* and *squares* are experimentally produced ol-plag-aug saturated melts and coexisting augites. The proportions of ol-plag-aug in fractionating assemblage are 0.08–0.45–0.47 which minimize the difference between the residual and predicted paths. *Arrows* indicate the directions of fractionation. The Ol-plag-aug fractionation terminates when the difference between residual melt and predicted OPALM is minimum. The *EMP error ellipse* is described in Fig. 5. The *dashed line* is the OPAM boundary predicted by the method of Grove et al. (1992)

## Comparison of predicted fractional crystallization sequences (FCS)

We carried out fractional crystallization models using composition ALV-2004-3-1, a high-MgO glass from East Pacific Rise (EPR). This composition was used for

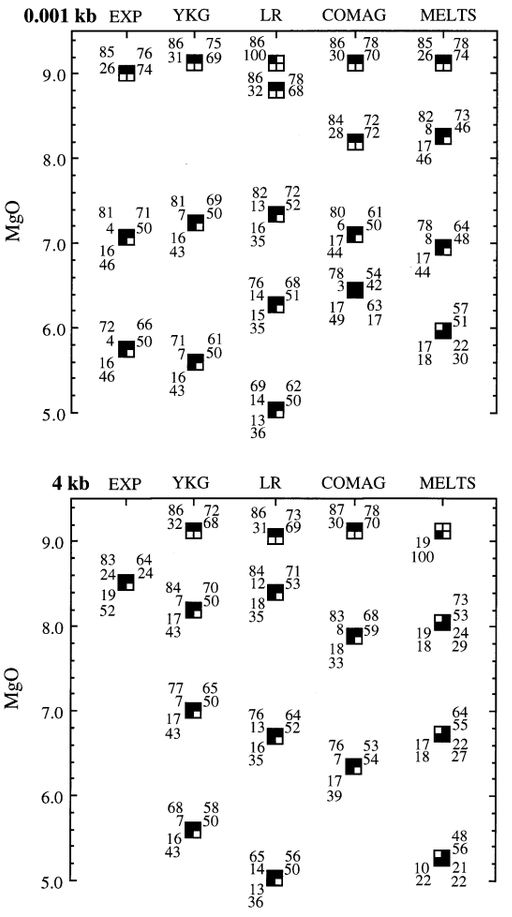


**Fig. 9** Comparison of predicted phase appearances with observed phase appearance for ALV-2004-3-1. Data for ALV-2004-3-1 are derived from Tables 2 and 3 and inferred from an 8 kbar experiment in Grove et al. (1992). For models and experiments the saturating phases are shown using the same symbols used in Fig. 1 with the exception of *lower right boxes* in MELTS (opx) and COMAG (spinel). *Numbers* next to each phase are the composition (*on top*: Fo of ol, An content of plag or MgO wt% of pyroxene) and the weight fraction in crystallizing assemblage (*below*). The MgO on vertical axis represents the MgO content of the experimental or predicted liquid

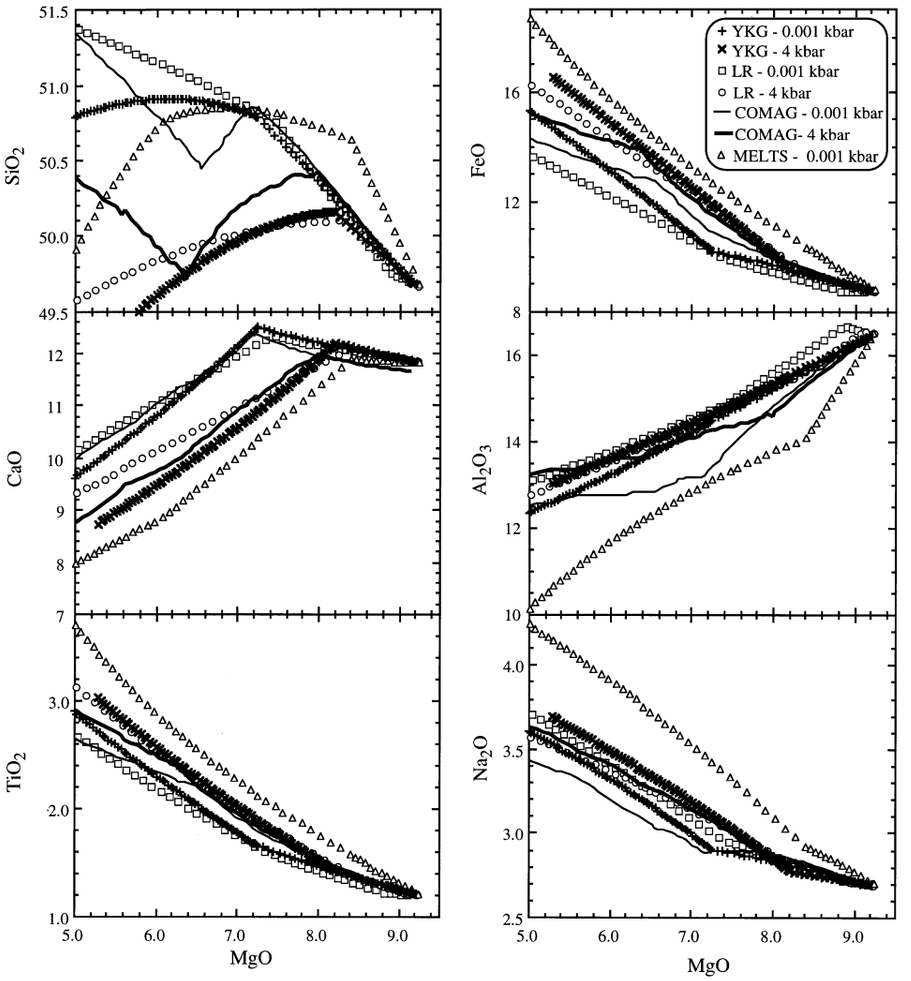


**Fig. 10** Fractional crystallization sequences starting from ALV-2004-3-1 calculated by the models of YKG (this paper), LR (Langmuir et al. 1992, modified by Reynolds 1995), COMAG (Ariskin et al. 1993) and MELTS (Ghiorso and Sack 1995). In YKG each increment is 1 wt% while in LR, COMAG and MELTS each increment is 2°C

the experimental study, and some aspects of these isothermal experiments can directly be compared with the FCS models. The models were calculated at 0.001 and 4 kbar, and include: the model presented in this paper (YKG), Langmuir et al. (1992) (with modifications by Reynolds 1995, referred as LR), Ariskin et al. (1993, COMAG) and Ghiorso and Sack (1995, MELTS). In each model fractional crystallization began at the liquidus and ceased at 5.00 wt% MgO. Results are summarized in Figs. 9, 10 and Table 7. First we compare the phase appearance sequence and proportions of near liquidus phases. In the case of basalt melts that are near multiphase saturation on their liquidi (ol-plag and ol-plag-aug in the case of ALV-2004-3–1) the differences between isothermal mineral phase appearance compositions and proportions and those that occur during fractional crystallization are small, so a comparison with the experimental data is justified. Second, we compare experimentally produced mineral compositions in an ol-plag-aug saturated melt with the phase compositions predicted for that liquid by the models. Third, we compare the liquid compositional variations followed during the fractional crystallization. In this instance, the isothermal experiments on ALV-2004-3–1 are not comparable, and only the models will be compared.

The 0.001 kbar crystallization sequences predicted from YKG, LR, COMAG and MELTS are illustrated in Fig. 9. Sample ALV-2004-3-1 has ol+plag on the liquidus and YKG and COMAG also predict these as liquidus phases. The models MELTS (not shown in Fig. 9, because temperature interval is small) and LR predict ol as a liquidus phase. Models YKG, LR and COMAG predict that augite joins the fractionating assemblage when residual melt evolves to 7.24, 7.46 and 7.16 wt% MgO, respectively. However, MELTS predicts that augite crystallizes at 8.39 wt% MgO and orthopyroxene crystallizes at 6.07 wt% MgO. In contrast to the prediction of MELTS, orthopyroxene is not observed in the experiments, nor is it a stable phase on the FCS calculated by YKG, LR and COMAG. Similarly, magnetite is not stable, but is predicted by COMAG. In summary, the early crystallization sequence predicted by MELTS, YKG, LR and COMAG are generally similar to the experimentally determined crystallization sequence, but there are some differences in later phase appearances. At 4 kbar, YKG predicts that ol and plag are liquidus phases, and the

**Table 7** Predicted mineral compositions in equilibrium with an experimentally produced ol-plag-aug saturated melt, ALV-2004-3-1-60. YKG, LR and MELTS indicate compositions predicted from the method presented in this study and those of Langmuir et al. (1992) (with modification by Reynolds, 1995), and Ghiorso and Sack (1995). *EXP* indicates experimentally determined mineral composition in equilibrium with ALV-2004-3-1-60 at 0.001 kbar (this study)

| | EXP | YKG | LR | MELTS |
|---|---|---|---|---|
| Fo | 75.2 | 74.1 | 74.1 | |
| An | 66.1 | 67.8 | 71.3 | 62.0 |
| Augite | | | | |
| $SiO_2$ | 51.8 | 52.02 | 52.52 | 51.06 |
| $TiO_2$ | 0.94 | 0.99 | 1.00 | 0.72 |
| $Al_2O_3$ | 2.46 | 2.78 | 2.59 | 4.15 |
| FeO | 7.94 | 8.00 | 7.61 | 10.05 |
| MgO | 16.4 | 16.77 | 15.30 | 16.76 |
| CaO | 19.8 | 19.17 | 20.67 | 16.98 |
| $Na_2O$ | 0.26 | 0.25 | 0.31 | 0.28 |

residual liquid becomes augite saturated at 8.20 wt% MgO. Model LR predicts olivine as the liquidus phase (not shown in Fig. 9) followed by plagioclase after a 4°C interval and augite appears at 8.39 wt% MgO. Model COMAG predicts ol +plag as the liquidus assemblage, augite crystallizes at 7.9 wt% MgO and magnetite appears at 6.29% MgO. The crystallization sequence predicted by MELTS at 4 kbar is aug−aug+plag−aug+plag+opx−aug+plag+opx+sp. From the experiments of Grove et al. (1992), ALV-2004-3-1 is inferred to saturate with ol+plag+aug on its 8 kbar liquidus. Thus, MELTS predictions that augite is on the liquidus and that olivine is absent as a crystallizing phase are incorrect. For this reason, the FCS modeled by MELTS at 4 kbar is not considered in the following discussion. In summary, the crystallization sequences at 4 kbar predicted by YKG, LR and COMAG are generally similar and they differ from that predicted by MELTS.

The ol:plag proportions predicted from the four models are slightly different, but close to the proportions measured in ALV-2004-3-1 (Fig. 9). The MELTS estimate is identical to that in the experiment, and the LR estimate is 6 wt% higher in olivine. The ol:plag:aug proportions at the first appearance of aug in ALV-2004-3-1 are 4:50:46. The COMAG estimate (6:50:44) comes closest at 0.001 kbar to the values measured in the isothermal experiment.

To compare the compositions of minerals that each model predicts as crystallizing phases we chose an experimental liquid, ALV-2004-3-1-60, produced at 0.001 kbar and saturated with ol, plag and aug (Table 3). Models YKG and LR predict ol, plag and aug as saturating phases. The MELTS and COMAG do not predict olivine as one of the saturating phases for the ALV-2004-3-1-60 liquid. The model MELTS predicts aug + plag and COMAG predicts orthopyroxene as the saturating phase. Models YKG and LR predict the same olivine compositions (Table 7). Predicted anorthite (An) contents in plagioclase are 0.68 (YKG), 0.71 (LR) and 0.62 (MELTS) (Table 7). Compared to those predicted by YKG and LR, the augite composition at 0.001 kbar modeled by MELTS has higher $Al_2O_3$ and FeO, and lower $SiO_2$, $TiO_2$, and CaO (Table 7). Plagioclase and augite compositions calculated by YKG fall between those predicted by LR and MELTS and are closer to experimental results (Table 7).

The FCS predicted from YKG, LR, COMAG and MELTS at 0.001 and 4 kbar are compared in Fig. 10. The different slopes defined by ol-plag saturated melts in the MgO-$Al_2O_3$ and MgO-$SiO_2$ plot reflect the slight differences in the ol-plag proportions predicted by the four models. More significant differences exist between the ol-plag-aug saturated compositions predicted by each model. The early appearance of augite in the FCS predicted by MELTS causes low CaO in residual melts (Fig. 10). The high $TiO_2$ in ol-plag-aug saturated melts modeled by MELTS is due to the low $TiO_2$ contents in augite predicted by MELTS. In general, the FCS calculated from MELTS at 0.001 kbar differs significantly from those calculated from YKG, LR and COMAG. At a given MgO content YKG, COMAG and LR predict lower $SiO_2$ and CaO, and higher FeO at 4 kbar relative to their respective 0.001 kbar FCS. The V-shaped pattern produced by COMAG at 0.001 and 4 kbar is caused by the appearance of magnetite as a crystallizing phase. Model LR predicts higher $Na_2O$ contents in augite at 4 kbar causing $Na_2O$ in residual melts to increase less steeply (Fig. 10) relative to YKG and COMAG.

## Glasses from EPR: an example of fractionation at 2 kbar

Glasses were collected with the submersible ALVIN from the east limb of the overlapping spreading center at 11°45′N on the EPR. Most of the samples have MgO ranging from 6∼7%. Detailed sampling localities and major element chemistry are described by Thompson et al. (1989). The data presented in Fig. 11 are from the MIT electron microprobe (Kinzler 1991), and therefore are not corrected for interlaboratory bias. In the Ol-Cpx-Qtz pseudoternary most of the dredged glasses form a coherent trend parallel to but offset towards olivine from the 0.001 kbar OPAM boundary defined by experimental data. Some glasses deviate from the coherent trend and plot even farther towards the olivine corner. These are potential parental compositions for glasses that fall on the trend paralleling the 0.001 kbar OPAM boundary. The first ol-plag-aug saturated melts predicted from 4 potential parental compositions at 2 kbar lie on the trend defined by most glasses (solid squares, Fig. 11). Therefore, the trend defined by most of the glasses can be explained by magmas evolving from different parents to the onset of ol-plag-aug crystallization at 2 kbar, and thus imply significant evolution by crystallization processes at the base of the oceanic crust on this segment of the EPR.

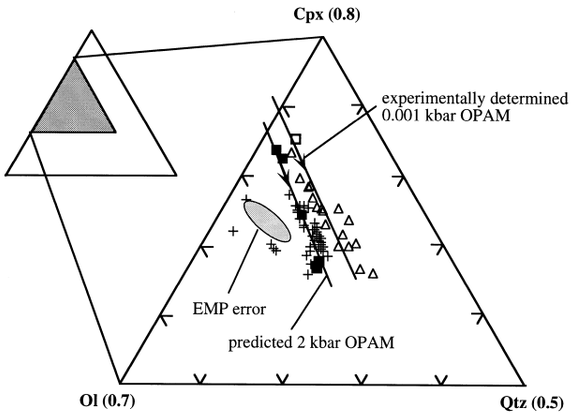


**Fig. 11** Comparison of glasses from east flank of EPR (*crosses*), experimentally produced ol-plag-aug saturated melts at 0.001 kbar (*open triangles*) and the first ol-plag-aug saturated melts predicted from five glasses, 2004-3-1, 2003-6-1, 2002-2-1, 2003-4-1 and 2004-2-1 at 2 kbar (*solid squares*). The first ol-plag-aug saturated melt at 0.001 kbar (*open square*) is predicted from 2004-3-1. *Two straight lines* are drawn by eye fit to the 0.001 kbar experimental results (Tables 2 and 3) and the predicted first ol-plag-aug saturated melts at 2 kbar. The *EMP error ellipse* is described in Fig. 5

**Acknowledgments** We thank G.A. Gaetani for his input into this study and help in laboratory work. S. Recca and M. Jercinovic are acknowledged for their assistance in electron microprobe analysis. We also thank Peter Keleman and Kwok-Lin Lee for running MELTS. The work benefited from discussions with T. Wagner, E. Takazawa and A. Saal. Reviews from F.A. Frey, P. Michael and R. Nielsen were very helpful. This research was supported by OCE-9415968 and OCE-9115901.

## References

Albee AL, Ray L (1970) Correction factors for electron microprobe analysis of silicates, oxides, carbonates, phosphates and sulfates. Anal Chem 42: 1408–1414

Ariskin AA, Frenkel MY, Barmina GS, Nielsen RL (1993) Comagmat: a FORTRAN program to model magma differentiation processes. Comput Geosci 19: 1155–1170

Baker DR, Eggler DH (1987) Composition of anhydrous and hydrous melts coexisting with plagioclase, augite, and olivine or low-Ca pyroxene from 1 atm to 8 kbar: application to Aleutian volcanic center of Atka. Am Mineral 72: 12–28

Bence AE, Albee AL (1968) Empirical correction factors for the electron microanalysis of silicates and oxides. J Geol 76: 382–403

Bender JF, Hodges FN, Bence AE (1978) Petrogenesis of basalts from the project FAMOUS area: experimental study from 0 to 15 kbar. Earth Planet Sci Lett 41: 277–302

Biggar GM (1972) Diopside, lithium metasilicate and the 1968 temperature scale. Mineral Mag 38: 768–770

Biggar GM, Humphries DJ (1981) The plagioclase, forsterite, diopside, liquid equilibrium in the system CaO-$Na_2O$-MgO-$Al_2O_3$-$SiO_2$. Mineral Mag 44: 309–314

Davidson PM (1985) Thermodynamic analysis of quadrilateral pyroxene. I. Derivation of the ternary non-convergent site-disorder model. Contrib Mineral Petrol 91: 383–389

Davidson PM, Lindsley DH (1985) Thermodynamic analysis of quadrilateral pyroxenes. II. Model calibration from experiments and applications to geothermometry. Contrib Mineral Petrol 91: 390–404

Gaetani GA, DeLong SE, Wark DA (1995) Petrogenesis of basalts from the Blanco Trough, Northeast Pacific: inferences for off-axis melt generation. J Geophys Res 100: 4197–4214

Gee LL, Sack RO (1988) Experimental petrology of melilite nephelinites. J Petrol 29: 1233–1255

Ghiorso MS, Sack RO (1995) Chemical mass transfer in magmatic processes. IV. A revised and internally consistent thermodynamic model for the interpolation and extrapolation of liquid-solid equilibria in magmatic systems at elevated temperatures and pressures. Contrib Mineral Petrol 119: 197–212

Grove TL (1981) Use of FePt alloys to eliminate the iron loss problem in 1-atmosphere gas mixing experiments: theoretical and practical considerations. Contrib Mineral Petrol 78: 298–304

Grove TL, Bryan WB (1983) Fractionation of pyroxene-phyric MORB at low pressure: an experimental study. Contrib Mineral Petrol 84: 293–309

Grove TL, Vaniman DT (1978) Experimental petrology of very low Ti (VLT) basalts. In: Mare Crisium: the View from Luna 24. Pergamon Press, New York, pp 445–471

Grove TL, Kinzler RJ, Bryan WB (1990) Natural and experimental phase relations of lavas from Serocki Volcano. Ocean Drill Proc Sci Results 106/109: 9–17

Grove TL, Kinzler RJ, Bryan WB (1992) Fractionation of mid-ocean ridge basalt (MORB). Am Geophys Union Geophys Monogr 71: 281–310

Grove TL (1993) Corrections to equations for calculating mineral components in "Origin of calc-alkaline series lavas at Medicine Lake Volcano by fractionation, assimilation and mixing" and "Experimental petrology of normal MORB near the Kane Fracture Zone: 22–25°N, mid-Atlantic ridge". Contrib Mineral Petrol 114: 422–424

Juster TC, Grove TL (1989) Experimental constraints in the generation of FeTi basalts, andesites, and rhyodacites at the Galapagos spreading center, 85°W and 95°W. J Geophys Res 94: 9251–9274

Kinzler RJ (1991) Experimental constraints on the generation and evolution of mid-ocean ridge basalts. PhD thesis, MIT, Cambridge, USA

Kinzler RJ, Grove TL (1992) Primary magmas of mid-ocean ridge basalts. 1. Experiments and methods. J Geophys Res 97: 6885–6906

Langmuir CH, Klein EM, Plank T (1992) Petrological systematics of mid-ocean ridge basalts: constraints on melt generation beneath mid-ocean ridges. Am Geophys Union Geophys Monogr 71: 183–280

Libourel G, Boivin P, Biggar GM (1989) The univariant curve liquid=forsterite + anorthite + diopside in the system CMAS at 1 bar: solid solutions and melt structure. Contrib Mineral Petrol 102: 406–421

Longhi J (1991) Comparative liquidus equilibria of hypersthene-normative basalts at low pressures. Am Mineral 76: 785–800

Nielsen RL, Davidson PM, Grove TL (1988) Pyroxene-melt equilibria: an updated model. Contrib Mineral Petrol 100: 361–373

Presnall DC, Dixon SA, O'Donnel TH, Brenner NL, Schrock RL, Dycus DW (1978) Liquidus phase relations on the join Diopside-Forsterite-Anorthite from 1 atm to 20 kbar: their bearing on the generation and crystallization of basaltic magma. Contrib Mineral Petrol 66: 203–220

Reynolds JR (1995) Segment-scale systematics of mid-ocean ridge magmatism and geochemistry. PhD thesis, Columbia Univ

Roeder PL, Emslie RF (1970) Olivine-liquid equilibrium, Contrib Mineral Petrol 29: 275–289

Sack RO, Carmichael ISE (1984) $Fe^{+2+}=Mg^{+2}$ and $TiAl_2=MgSi_2$ exchange reactions between clinopyroxene and silicate melts. Contrib Mineral Petrol 85: 103–115

Sack RO, Walker D, Carmichael ISE (1987) Experimental petrology of alkalic lavas: constraints on cotectics of multiple saturation in natural basic liquids. Contrib Mineral Petrol 96: 1–23

Shi P (1992) Basalt evolution at low pressure: implications from an experimental study in the system CaO-FeO-MgO-$Al_2O_3$-$SiO_2$. Contrib Mineral Petrol 110: 139–153

Shi P (1993) Low-pressure phase relationships in the system $Na_2O$-CaO-FeO-MgO-$Al_2O_3$-$SiO_2$ at 1100ºC, with implications for the differentiation of basaltic magmas. J Petrol 34: 743–762

Shi P, Libourel G (1991) The effect of FeO on the system CMAS at low pressure and implications for basalt crystallization processes. Contrib Mineral Petrol 108: 129–145

Stolper E (1980) A phase diagram for mid-ocean ridge basalts: preliminary results and implications for petrogenesis. Contrib Mineral Petrol 74: 13–27

Thompson G, Bryan WB, Ballard RD, Hamuro K, Melson WG (1985) Axial processes along a segment of the East Pacific Rise, 10–12°N. Nature 318: 429–433

Thompson G, Bryan WB, Humphris SE (1989) Axial volcanism on the East Pacific Rise, 10–12°N. In: Saunders AD, Norry MJ (eds) Magmatism in the oceanic basins. Geol Soc Spec Publ 42

Tormey DR, Grove TL, Bryan WB (1987) Experimental petrology of normal MORB near the Kane Fracture Zone: 22–25°N, mid-Atlantic ridge. Contrib Mineral Petrol 96: 121–139

Ulmer P (1989) The dependence of the $Fe^{2+}$-Mg cation-partitioning between olivine and basaltic liquid on pressure, temperature and composition. An experimental study to 30 kbar. Contrib Mineral Petrol 101: 261–273

Walker D, Shibata T, DeLong SE (1979) Abyssal tholeiites from the Oceanographer fracture zone. II. Phase equilibria and mixing. Contrib Mineral Petrol 70: 111–125

Walter MJ, Presnall DC (1994) Melting behavior of simplified lherzolite in the system CaO-MgO-$Al_2O_3$-$SiO_2$-$Na_2O$ from 7 to 35 kbar. J Petrol 35: 329–359